Geochemistry, Geophysics, Geosystems®

RESEARCH ARTICLE
10.1029/2021GC010112

Regional Geophysics of the Caribbean and Northern South America: Implications for Tectonics

Carol V. Barrera-Lopez[1], Walter D. Mooney[1], and Mikhail K. Kaban[2]

[1]Earthquake Science Center, United States Geological Survey, Menlo Park, CA, USA, [2]Helmholtz-Centre Potsdam – GFZ German Research Centre for Geosciences, Potsdam, Germany

Key Points:

- A new crustal thickness map and gravity maps reveal large areas of normal-thickness oceanic crust within the Caribbean plate
- P-wave seismic tomography images show that the subducted Caribbean plate reaches 660 km depth, but slab seismicity terminates at 200 km
- Combined seismicity, gravity, and magnetic maps reveal the active tectonics of the circum-Caribbean accretionary and magmatic boundary

Supporting Information:

Supporting Information may be found in the online version of this article.

Correspondence to:

C. V. Barrera-Lopez,
cv.barrera10@uniandes.edu.co

Citation:

Barrera-Lopez, C. V., Mooney, W. D., & Kaban, M. K. (2022). Regional geophysics of the Caribbean and northern South America: Implications for tectonics. *Geochemistry, Geophysics, Geosystems*, *23*, e2021GC010112. https://doi.org/10.1029/2021GC010112

Received 25 AUG 2021
Accepted 1 MAY 2022

Author Contributions:

Conceptualization: Carol V. Barrera-Lopez, Walter D. Mooney
Formal analysis: Carol V. Barrera-Lopez, Walter D. Mooney
Investigation: Carol V. Barrera-Lopez, Walter D. Mooney
Methodology: Carol V. Barrera-Lopez, Walter D. Mooney, Mikhail K. Kaban
Project Administration: Walter D. Mooney
Resources: Walter D. Mooney
Software: Mikhail K. Kaban

Abstract The Caribbean plate is an enclosed oceanic basin whose formation and evolution are controversial. In the most commonly accepted model, the Caribbean plate is mainly composed of the Caribbean Large Igneous Province (CLIP) and the buoyant characteristic of this oceanic plateau resisted subduction and allowed an eastward migration to its present position north of South America. In this study, we integrate a broad range of geophysical and geomorphological data to define structural elements and present-day tectonics of the Caribbean plate and the surrounding region. We present a Bouguer gravity anomaly map and a new crustal thickness map that documents large areas of normal-thickness oceanic crust within the Venezuela and Colombia basins of the Caribbean plate. Selected cross sections of seismicity and P-wave anomalies from a seismic tomographic model depict the present-day geometry of subducting oceanic plates within the Caribbean region. We observe that rather than resisting subduction, as expected for the thick crust of a buoyant large igneous province, the subduction of the Caribbean plate can be traced to a depth of 600 km beneath NW South America. This, together with the crustal thickness map, implies that a significant area of the Caribbean plate, including the subducted portion, is composed of normal-thickness oceanic crust. As proposed by the Pacific origin model, the Caribbean plate likely migrated eastward from the Pacific Ocean as an oceanic plate mostly with normal-thickness crust and limited portions of the crust thickened by hot spot volcanism (CLIP).

Plain Language Summary The Caribbean plate and northern South America are studied using topography and multiple geophysical data sets, including gravity, magnetics, crustal thickness, seismicity, and seismic images of the upper mantle. These data sets were used to analyze crustal properties as well as the past and present interaction of tectonic plates in this region. Our results show large areas of ocean crust with normal thickness within the Caribbean plate. Seismicity in the circum-Caribbean subduction zones rarely exceeds 200 km in depth, whereas seismic imaging shows subducting slabs reach a depth of 600 km or more. This implies that subduction has been long-lived at these active margins. These results also show that the Caribbean plate is subducting beneath NW South America, something that would not be expected for the thick crust of a buoyant large igneous province. As proposed by the Pacific origin model, the Caribbean plate migrated eastward from the Pacific Ocean as an oceanic plate mostly with normal-thickness crust and limited portions of the crust thickened by hot spot volcanism.

1. Introduction

The structure and tectonics of the Caribbean and northern South America have been extensively studied since the 1950s (Ewing et al., 1960; Hess & Maxwell, 1953; Meyer et al., 1976). Five tectonic plates converge in this region: the South American, North American, Nazca, Cocos, and Caribbean plates (Figure 1). Whereas the evolution of the first four of these plates is well understood, the origin of the Caribbean plate is the subject of considerable debate (Burke et al., 1978; James, 2006; Pindell & Dewey, 1982).

There are two main competing hypotheses for the origin of the Caribbean plate. These are termed the in situ origin (James, 2006) and the Pacific allochthonous origin (Burke et al., 1978; García-Reyes & Dyment, 2021; Pindell & Dewey, 1982). The first hypothesis, also referred to as the "Intra-Americas model," argues that the Caribbean plate originated between the North and South American plates from an episode of decompression melting in the Aptian (125–113 Ma; James, 2006). In the second hypothesis, the Caribbean plate originated in the Late Cretaceous as a large igneous province on the Farallon plate (Pacific) due to hot spot magmatism (Figures 2a and 2b; Burke et al., 1978; van Benthem et al., 2013). Following its formation, the Caribbean Large Igneous Province (CLIP) migrated eastward to its present position between North and South America (Figures 2c and 2d).

Supervision: Carol V. Barrera-Lopez, Walter D. Mooney
Visualization: Mikhail K. Kaban
Writing – original draft: Carol V. Barrera-Lopez
Writing – review & editing: Carol V. Barrera-Lopez, Walter D. Mooney

Currently, the Pacific origin of the Caribbean plate is the most commonly accepted model as it is in broad agreement with the available geophysical and geological evidence. The purpose of this article is to integrate a broad range of geophysical data to define the present-day structure and tectonics of the Caribbean plate and the surrounding region and to comment on its evolution. To achieve this objective, we present a new map of the crustal thickness of the region, interpret gravity, and magnetic data and define the geometry of subducting oceanic lithosphere based on seismicity and mantle tomography.

2. Tectonic Setting

Most of the models proposing the tectonic evolution of the region start with the rifting of western Pangea in the late Triassic that creates the Proto-Caribbean seaway (Figure 2a) between North and South America (Lugo & Mann, 1995; see also Gomez et al., 2018; Pindell & Kennan, 2009). Early Cretaceous subduction of the Farallon plate beneath the Proto-Caribbean oceanic crust created the Great Arc of the Caribbean (GAC; Pindell et al., 1988; Figure 2a).

The relative motion of the Caribbean plate with respect to the Americas has been accommodated by strike-slip faulting at its northern and southern boundaries (sinistral and dextral, respectively) and by subduction at its eastern and western boundaries. It is estimated that there has been around 1,100 km of west-to-east motion of the Caribbean plate since the middle-late Eocene (Mann, 1999; Pindell & Kennan, 2009). This plate motion has led to the accretion of oceanic plateau and arc segments along the northwestern South American margin (Montes et al., 2019). It has also created: (a) the South Caribbean Deformed Belt (Figures 2d and 2b), a strike-slip motion on the San Sebastian-El Pilar (SSEP) fault system (Figure 1) in northeastern Venezuela (Pindell et al., 1988; see also Kerr et al., 2003; Mann, 1999).

The present-day Caribbean plate is postulated to have formed within the Farallon plate in the late Cretaceous (100–80 Ma) by hot spot volcanism resulting in the CLIP (Figure 2b; Burke et al., 1978). The arrival of the buoyant CLIP at the trench in front of the GAC in the late Campanian (~75 Ma; Figure 2b) caused the subduction to flip to the eastern side of the GAC (Pindell et al., 1988) and slab rollback resulted in the insertion of the Caribbean plate between North and South America (Figure 2b; Gomez et al., 2018; Pindell et al., 1988). Since this time, the Caribbean plate has continued to migrate eastward with respect to the Americas (Mann, 1999; Pindell et al., 1988) as depicted in Figures 2c and 2d.

The oceanic lithosphere of the equatorial Atlantic is subducting at the eastern and northeastern margins of the Caribbean plate (van Benthem et al., 2013). The subduction and slab rollback of this lithosphere have created three key features in the Caribbean plate (Mann, 1999): (a) the Aves ridge, a remnant arc at the eastern side of the Venezuela basin that was active between 90 and 55 Ma (Christeson et al., 2008); (b) the Lesser Antilles Arc (currently active); and (c) the Grenada and Tobago basins (Figure 1). The western side of the Caribbean plate is bounded by southern Central America and is separated from the Colombia basin by the linear NE-SW Hess Escarpment. This escarpment is the eastern margin of the Nicaraguan Rise and has been interpreted as an extension of the continental Chortis block from northern Central America to Jamaica and as a Neogene strike slip feature (Figure 1; Mann, 1999; see also Carvajal-Arenas & Mann, 2018).

The fragmentation of the southern Farallon plate into the Cocos and Nazca plates took place in the late Oligocene (Pindell et al., 1988). Multiple structures developed as the Cocos plate moved northeast, while the Nazca plate moved east: (a) The N-S spreading in the Galapagos rift was initiated, (b) the Caribbean—Nazca—Cocos triple junction, and (c) the Carnegie and Cocos ridges, which recorded the motion of the plates over the Galapagos hot spot (Figure 2d; Smith, 1985; Gutscher et al., 1999). Plate motion models suggest that the Malpelo ridge is the northern section of the Cocos ridge that was shifted due to the N-S dextral strike-slip boundary between the Cocos and Nazca plates (Gutscher et al., 1999; Hey et al., 1977).

3. Data Sources

This paper uses multiple geophysical data sets in order to sample a range of physical properties and depths from crustal levels to the lower mantle. This is particularly appropriate because the study area is one with long-lived subduction with oceanic lithosphere that can be imaged to depths greater than 1,000 km (Simmons et al., 2012; van Benthem et al., 2013; Zhu et al., 2020). The scientific value of a multidisciplinary approach to structural

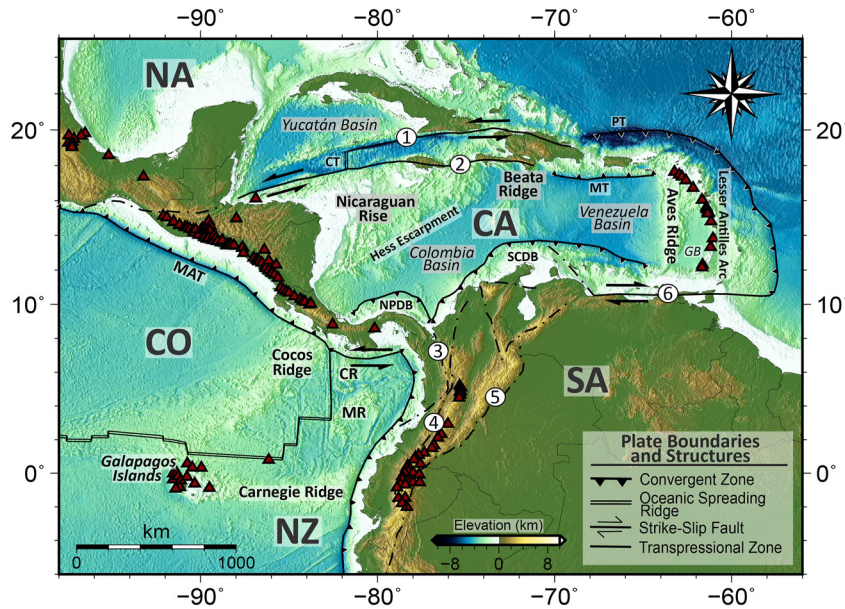

Figure 1. Tectonic map of the Caribbean and northern South America region. Red triangles are Holocene volcanoes (Global Volcanism Program, 2013). Abbreviations for tectonic plates are CA—Caribbean Plate, CO—Cocos Plate, NZ—Nazca Plate, NA—North American Plate, SA—South American Plate. Tectonic structures: CR—Coiba Ridge, CT—Cayman Trough, GB—Grenada Basin, MR—Malpelo Ridge, MAT—Middle American Trench, MT—Muertos Trough, NPDB—North Panama Deformed Belt, PT—Puerto Rico Trench, SCDB—South Caribbean Deformed Belt. Main Faults (F) and Fault Systems (FS): 1. Septentrional-Oriente FS; 2. Enriquillo-Plantain-Garden F; 3. Uramita FS; 4. Romeral FS; 5. Guaicaramo FS; 6. San Sebastian—El Pilar FS.

and tectonic studies in this region is well documented (Bernal-Olaya et al., 2015; Finger et al., 2021; Romito & Mann, 2020).

The regional free-air gravity anomaly grid was obtained from Sandwell et al. (2014). This grid is a global gravity model that combines new radar altimeter measurements from satellites, CryoSat-2 and Jason-1, with previous data to obtain a model that is twice as accurate as previous gravity models (Sandwell et al., 2014). Examples of the use of gravity data for tectonic studies in the Caribbean and northern South America are presented in Bernal-Olaya et al. (2015), Gómez-García et al. (2019), Kellogg et al. (1995), Romito and Mann (2020), and Finger et al. (2021).

The magnetic anomaly model used is the third version of the Earth Magnetic Anomaly Grid at 2 arc-minute resolution (EMAG2v3). This magnetic model is compiled from marine and airborne magnetic measurements, and the satellite-derived Magnetic Field Model MF7 produced using CHAMP measurements from May 2007 to April 2010. This version has a data-only approach, which avoids the generation of artificial linear patterns along oceanic spreading ridges (Meyer et al., 2017).

A database of 1D models for the seismic velocity structure of the crust and the uppermost mantle of the study area were extracted from published reports (Data Set S1). These seismic models were compiled from multiple publications that derived them from two primary methodologies, namely active source (i.e., refraction and reflection profiling) and passive source (i.e., analysis of receiver functions and tomography; Mooney, 2015). This database was used to calculate the crustal thickness of the study area. A detailed description of the database of seismic crustal structure measurements for South America is provided by Chulick et al. (2013).

Earthquake locations for all events of $M \geq 4$ were obtained from the reviewed International Seismological Centre Bulletin for the time period 1 January 2005 to 30 April 2019 (International Seismological Centre, 2021). Focal mechanisms from the Global Centroid Moment Tensor Catalog (Ekström et al., 2012) were downloaded for earthquakes of $M \geq 6$ and greater from 1976 to 2020. This magnitude was selected as it provides a sufficient number of reliable focal mechanisms (cf., Hutchings & Mooney, 2021). The relative plate motion vectors are from the NNR-MORVEL56 model (Argus et al., 2011).

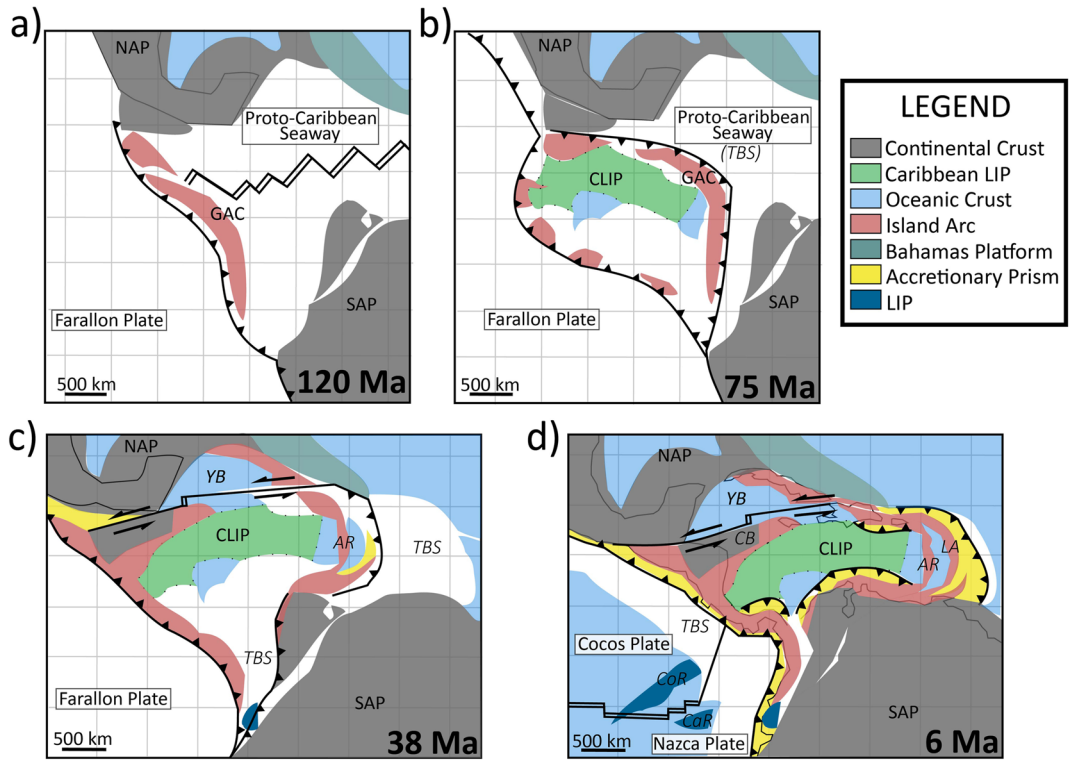

Figure 2. Schematic tectonic evolution of the Caribbean and northern America regions modified from Gomez et al. (2018) and Romito and Mann (2020). (a) At 120 Ma (Early Cretaceous), the Great Arc of the Caribbean (GAC) was already developed due to the subduction of the Farallon plate beneath the Proto-Caribbean Seaway. (b) At 75 Ma (Campanian), the Caribbean Large Igneous Province (CLIP; size and shape unknown) formed in the Late Cretaceous (~80 Ma) and collided with the GAC, triggering a reversal of the subduction due to its buoyancy. (c) At 38 Ma (Bartonian), the collision of the northeastern segment of the CLIP with the Bahamas Platform reoriented the motion of the plate toward the east, which initiated a pull-apart regime in the Yucatan basin in the Paleocene that migrated to the Cayman trough in the Eocene; magmatism migrated to the east leaving the Aves Ridge, a remnant arc, and generating the Lesser Antilles volcanic arc. (d) From 38 to 6 Ma, the Farallon plate was fragmented into the Cocos and Nazca plates and the Cocos and Carnegie ridges (Large Igneous Provinces—LIP) started to form due to the interaction of the plates with the Galapagos hotspot; convergence of the CLIP with the northern South America created the SDCB and NPDB. Abbreviations: TBS—areas to be subducted, CB—Chortis block.

The seismic tomography cross sections are taken from the model DETOX-P1 (Hosseini et al., 2020) and were obtained from the "SubMachine" tomography web portal (Hosseini et al., 2018). The DETOX-P1 model is based on 2.5 million teleseismic P-wave travel times (Hosseini et al., 2020) and it is the preferred model to study the upper half of the mantle as the resolution of subducted lithosphere is higher and the anomalies are less affected by smearing artifacts (Mohammadzaheri et al., 2021).

4. Methods and Analysis

4.1. Gravity Anomaly

To obtain insights into the sources of the density anomalies and facilitate geological interpretations, the calculation of the simple Bouguer and residual gravity anomalies was performed following the equations given by Blakely (1995) as described below.

4.1.1. Simple Bouguer Anomaly

The simple Bouguer anomaly (Figure 3a) was calculated using density values of 2.67 g/cm^3 onshore and 1.645 g/cm^3 offshore (2.67 g/cm^3 of the crust minus 1.025 g/cm^3 of the water) as presented by Barthelmes (2009). This correction does not consider the low-density root that supports the topography on continents; therefore, positive anomalies are expected over oceanic areas and negative anomalies over continents (Blakely, 1995). Bouguer

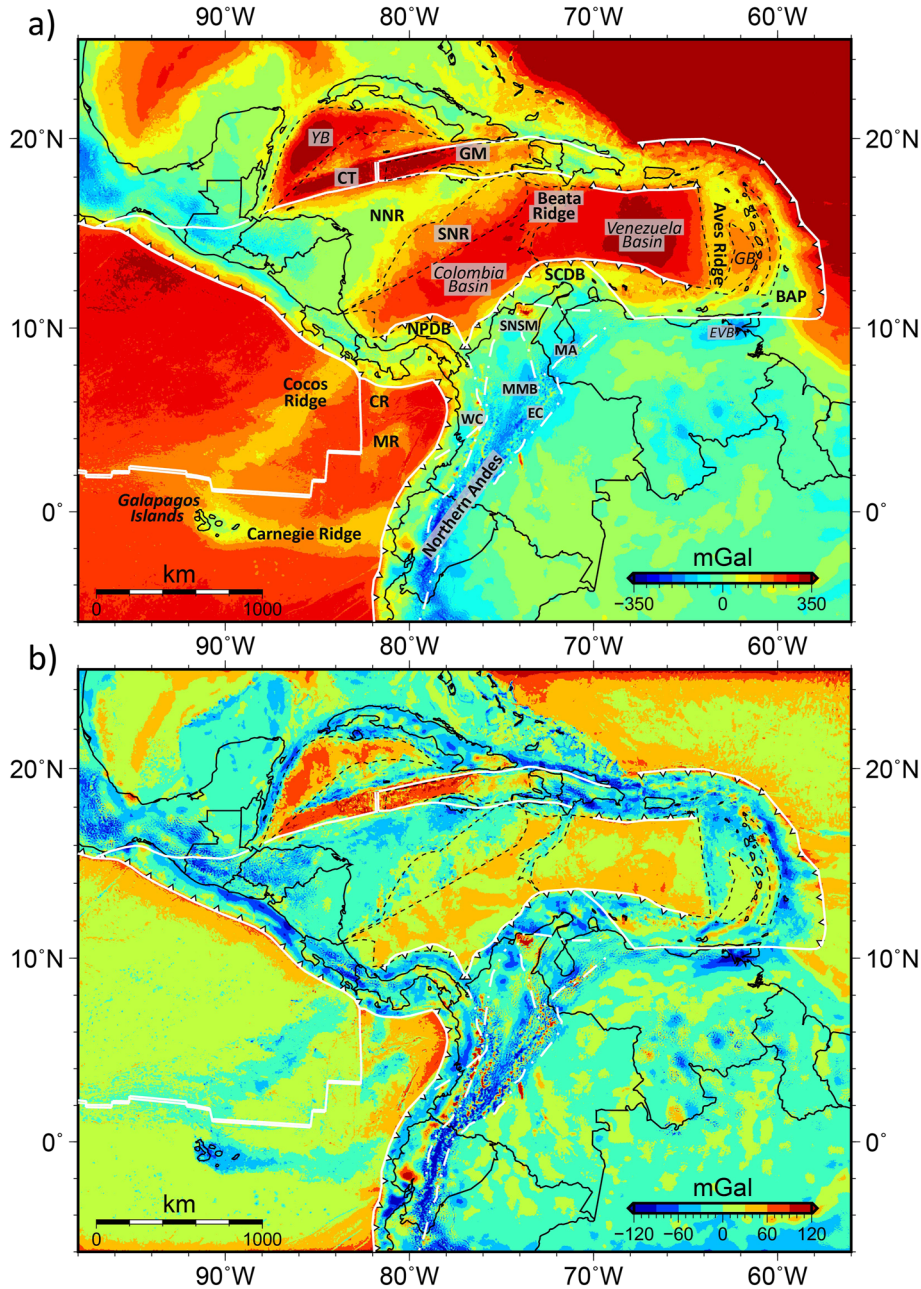

Figure 3. Gravity anomalies of Central and South America from Sandwell et al. (2014). (a) Simple Bouguer Anomaly. Warmer colors (reds) are generally related to a thinner crust than colder (blue) colors. Dashed lines are tectonic/terrane boundaries defined by Gómez-García et al. (2019). Abbreviations: NNR—Northern Nicaraguan Rise, SNR—Southern Nicaraguan Rise, EVB—Eastern Venezuela Basin, BAP—Barbados Accretionary Prism, GM—Gonave Microplate, WC—Western Cordillera, MMB—Middle Magdalena Basin, EC—Eastern Cordillera, MA—Mérida Andes, and SNSM—Sierra Nevada of Santa Marta. (b) Residual Anomaly. Emphasizes shallow (0–50 km) density anomalies. Overall, the oceanic domain has positive residual anomaly values and continental-related terrains have negative values. The Yucatan basin (YB) and Cayman Trough (CT) have high positive values of residual anomaly possibly due to a very thin sediment layer.

gravity anomalies within the study area have previously been described by Rodriguez-Millan (2014), Bernal-Olaya et al. (2015), and Finger et al. (2021). Over continental areas, the minimum Bouguer gravity anomaly values (<−150 mGal) are found along the northern Andes (Figure 3a). This pronounced gravity low (−346 mGal minimum value) has a NNE-SSW trend and extends from Ecuador through the Eastern Cordillera and the middle Magdalena Basin in Colombia up to the Merida Andes of Venezuela (Figure 3a). We infer that these negative

values could be due to the thickened crust caused by Andean mountain building in NW South America that has been ongoing since the Cretaceous as proposed by Montes et al. (2019). In northeastern Venezuela, we interpret a negative Bouguer gravity anomaly related to the Eastern Venezuela Basin (Figure 3a). This basin has been previously interpreted as an Early Miocene foredeep, and the gravity anomaly has been associated with the loading of the terranes and deformed belt as a result of the oblique collision of the southeastern Caribbean plate with the northeastern South America plate (Castillo & Mann, 2021; Pindell, 1991; Rodriguez-Millan, 2014).

In the oceanic domain, the minimum Bouguer gravity anomaly values are prominent: (a) along the Cenozoic accretionary prisms (South Caribbean and North Panama deformed belts, SCDF and NPDF, respectively) as well as the Barbados accretionary prism (BAP; Figure 3a) and (b) on the Nicaraguan Rise with a significant difference between the northern Nicaraguan rise (NNR) and the southern Nicaraguan rise (SNR; Figure 3a). Maximum values typical of oceanic crust (greater than 300 mGal) are found in the Yucatan basin (YB), the Cayman Trough (CT), beneath the Atlantic Ocean, in a broad region within the Venezuela basin and in limited areas in the Colombia basin (Figure 3a). The Atlantic Ocean has the maximum Bouguer anomaly value (+447 mGal), potentially due to the presence of mafic oceanic crust underlain by cold and dense ~200 Ma old lithosphere (Boschman et al., 2014).

4.1.2. Residual Anomaly

The residual gravity anomaly (Figure 3b) is used to emphasize shallow density anomalies and is calculated with a two-step procedure. The first step is the upward continuation of the simple Bouguer anomaly to a height of 40 km. The upward-continued Bouguer gravity has strongly attenuated short-wavelength signals that are mainly produced by near-surface sources, whereas the relatively long-wavelength anomalies caused by deeper structures are unattenuated (Blakely, 1995). The upward continued gravity was removed from the initial grid, leaving behind the residual Bouguer anomaly map primarily containing short-wavelength anomalies. This method is equivalent to a discrete vertical derivative. It is used instead of a true vertical derivative because it results in a cleaner, less noisy anomaly map. Other studies within the region have also applied this method to calculate the residual gravity anomaly (Bernal-Olaya et al., 2015; Sanchez et al., 2016).

Thick, dense oceanic plateau slices and/or Cretaceous arc (GAC) fragments were accreted to the continental margin according to Kerr et al. (2003) (see also Escuder-Viruete et al., 2013; Vence & Mann, 2020); these units may be correlated with positive anomalies in the residual gravity map (Figure 4). In Central and South America, these positive residual anomalies (up to 120 mGal) are observed over the Nicoya peninsula (No. 1 in Figure 4a), Panamá and northwestern Colombia (Nos. 2, 3, and 4 in Figure 4a), part of the Western Cordillera (No. 5 in Figure 4a), and at the islands of Aruba and Curaçao (No. 6 and 7 in Figure 4b, respectively). In Hispaniola, the Duarte and Dumisseau Formations (No. 8 and 9 in Figure 4b) are also characterized by positive residual anomalies (30–60 mGal). These nine geologic units are all oceanic plateau rocks and/or GAC fragments inferred by geochemical analysis (Kerr et al., 2003) that is used to define the affinity (i.e., oceanic plateaus, arc fragments, plutons, or Proto-Caribbean ocean crust) of the basaltic rocks in the region. Boschman et al. (2014) and Kerr et al. (2003) associate the positive gravity anomalies in southern Cuba (Figure 4c) with Cretaceous island-arc rocks (GAC) and ophiolite complexes. Escuder-Viruete et al. (2013) propose that fragments of the GAC can also be found in a segment of the northern Caribbean accretionary complex in the Dominican Republic (Escuder-Viruete et al., 2013). Positive anomalies along the northern continental margin of Colombia may also be related to the GAC (Kroehler et al., 2011; Vence & Mann, 2020).

4.2. Magnetic Anomaly

Strong variations of the magnetic anomalies can be seen throughout the Caribbean region (Figure 5). Within the Caribbean plate, the lineaments are chaotic through the Colombia and Venezuela basins (Figure 5) although some W-E and SW-NE lineaments, respectively, could be interpreted (Christofferson, 1973; García-Reyes & Dyment, 2021). This is similar at the northern side of the Cocos and Nazca plate except around the Galapagos spreading center where clear magnetic stripes could be interpreted. Broad magnetic high and low anomalies can be found at the MAT, the Panama isthmus, and NW South America, as well as the boundary between the Bahamas platform and the Atlantic ocean, but not at the eastern margin of the Caribbean plate (Lesser Antilles or BAP; Figure 5).

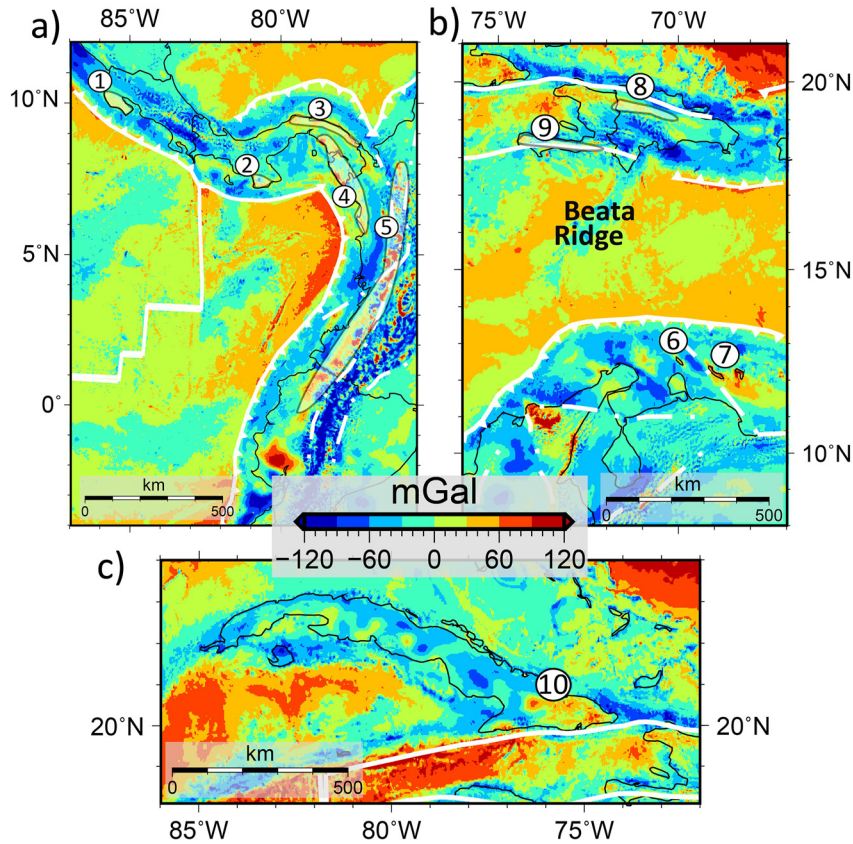

Figure 4. Mafic (high-density) accreted terranes interpreted in the residual anomaly map. Oceanic plateau and Cretaceous arc accreted terranes (Kerr et al., 2003; see also Escuder-Viruete et al., 2013; Vence & Mann, 2020): (a) 1. Nicoya peninsula, 2. Sona and Azuero, 3. Darien, 4. Serrania de Baudó, and 5. Western Cordillera. (b) 6. Aruba, 7. Curaçao, 8. Duarte formation, and 9. Dumisseau formation. (c) 10. Mayarí-Baracoa, an ophiolite complex (Boschman et al., 2014).

4.3. Crustal Thickness

Our analysis of crustal thickness began with 1,313 1D seismic velocity-depth models for the Caribbean and northern South America extracted from the global crustal database of Mooney (2015). Each seismic model describes the crustal structure with layers (i.e., sediment, crystalline crust, and uppermost mantle) of variable thicknesses and P- and S-wave seismic velocities. We adopted a P-wave velocity greater than 7.6 km/s as the crust-mantle (Moho) boundary (Mooney, 2015). Many of the 1D velocity models encompass only the crust and do not reach the Moho. After we removed these models, we retained 734 measurements of crustal thickness.

We found a scarcity of data for the eastern Pacific and South America in the global database. In order to fill these data gaps, we added velocity models obtained from seismic refraction/wide-angle reflection surveys ("seismic refraction data") carried out along the Galapagos spreading center (Canales et al., 2002) and the Carnegie ridge (Sallarès et al., 2005). We also added crustal measurements from receiver function studies over NW South America (Poveda et al., 2015), Venezuela (Mazuera et al., 2019), Peru (Condori et al., 2017), and Brazil (Albuquerque et al., 2017). Although the seismic refraction and receiver function methods differ, both methods are reliable in defining the depth to the Moho discontinuity, assuming good quality data. Refraction data contain high-amplitude wide-angle reflections from the Moho, whereas receiver functions have clear P-wave to S-wave conversions from the Moho. Hence, consistent measurements of crustal thickness are obtained when combining these results. The final database has 811 points (Figure 6; Data Set S1).

Controlled-source, reversed seismic refraction/wide-angle reflection data accounted for around 52% of the data set used. This method yields the most reliable measurements of crustal thickness for several reasons: (a) the source locations and shot times are precisely known; (b) the temporary seismographs are closely spaced along profiles with a nearly linear geometry; (c) seismic amplitudes as well as travel times are modeled during

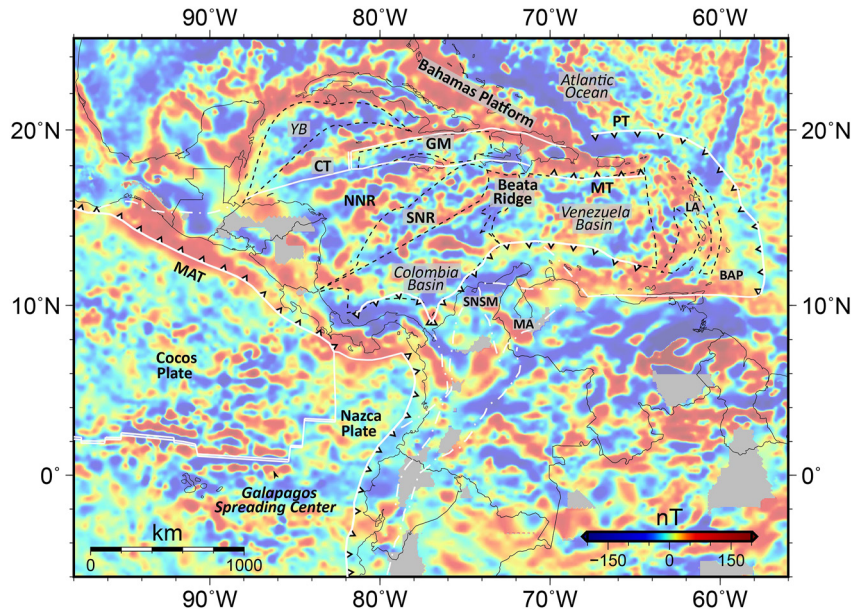

Figure 5. Magnetic anomaly map from EMAG2v3 (Meyer et al., 2017). Dashed lines are tectonic/terrane boundaries defined by Gómez-García et al. (2019). Abbreviations: YB—Yucatán Basin, CT—Cayman Trough, GM—Gonave Microplate, NNR—Northern Nicaraguan Rise, SNR—Southern Nicaraguan Rise, PT—Puerto Rico Trench, MT—Muertos Trough, LA—Lesser Antilles, BAP—Barbados Accretionary Prism, MA—Mérida Andes, SNSM—Sierra Nevada of Santa Marta, and MAT—Middle American Trench.

data interpretation; and (d) the reversed measurements from multiple sources provide overlapping subsurface rays coverage (Mooney, 2015). The remaining data consist primarily of passive-source methods like waveform models, receiver function analyses, tomography, and controlled-source measurements using unreversed refraction and split-spread geometry (Figure 6).

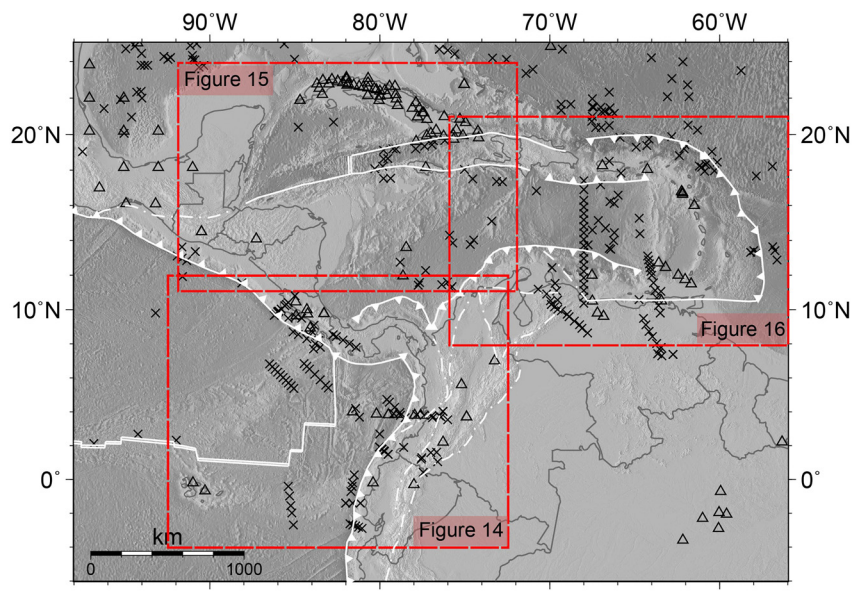

Figure 6. Locations of 1D seismic velocity-depth functions obtained from Mooney (2015), augmented with additional crustal models (see Text S1 in Supporting Information S1 and Data Set S1). Symbols denote the method used for the seismic survey. Crosses: Active-source seismic methods; Triangles: passive-source seismic methods.

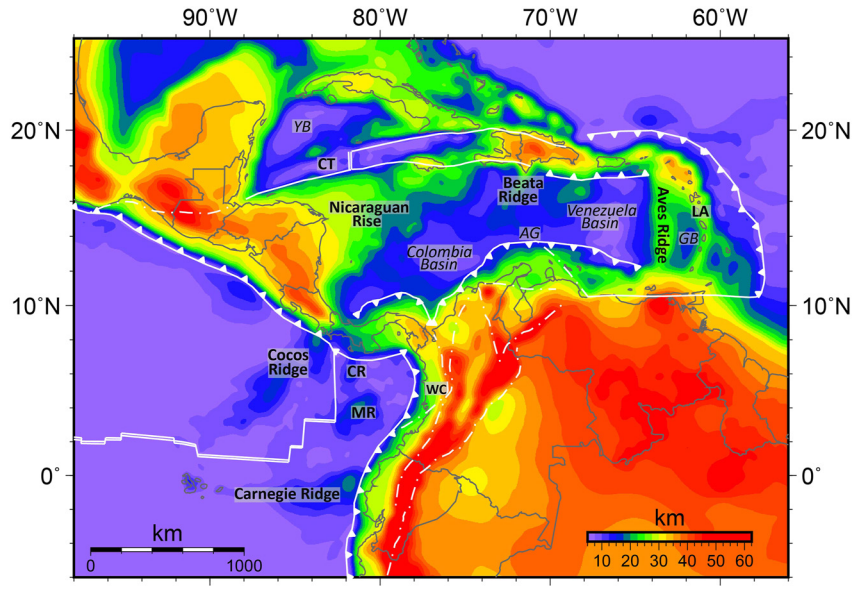

Figure 7. Crustal thickness map (including sediments and topography) of the Caribbean and northern South America. Oceanic crust with normal thickness (6–8 km) within the Caribbean region is found in the Yucatan basin (YB), the Cayman trough (CT), and a small segment between the Beata ridge and the Nicaraguan rise. In addition, a wide region that covers most of the Venezuela basin to the west, narrows at the Aruba gap (AG), and continues to the eastern segment of the Colombia basin also has a normal thickness for an oceanic crust. Oceanic crust with the normal thickness is also found within the Cocos and Nazca plates and under the Atlantic Ocean, except under aseismic ridges. A very thin crust is found at the Western cordillera (WC).

Since the available seismic measurements are unevenly distributed, their direct interpolation would result in a map with many artifacts, a common difficulty for irregularly distributed data. Stolk et al. (2013) introduced the so-called "remove-compute-restore" method that yields a much improved estimate of the Moho contours. The key to this method is also to consider the topography when interpolating the Moho depth values. The first step is the calculation of the adjusted topography (h-adjusted), representing the topography if water and sediments were numerically converted to a standard density 2.67 g/cm^3:

$$h_{\text{adj}} = t + w\frac{1.03}{2.67} - s\frac{\rho_{\text{sed}}}{2.67} \tag{1}$$

where t is the topography/bathymetry, w is the thickness of water, s is the thickness of sediments, ρ_{sed} is the vertically averaged density of sediments, 1.03 g/cm^3 is the density of water, and 2.67 g/cm^3 is the normal density of the upper crust. The data on the sediments thickness and density are taken from Mooney and Kaban (2010), Tesauro et al. (2014), and Finger et al. (2021).

Thus, the adjusted topography represents a homogeneous surface load. In the second step, preliminary Moho depths are calculated assuming Airy isostasy for compensation of the adjusted topography. It has been assumed that the difference of the upper-mantle density and average density of the crystalline crust is equal to 0.47 g/cm^3 (e.g., Mooney & Kaban, 2010). After removing these depths from the seismically determined ones, the "residual" Moho is calculated. The residual Moho has a lower RMS than the observed one and therefore is more appropriate for interpolation (Stolk et al., 2013).

The initial seismic data may contain some errors or small local deviations, which can significantly bias the map that is based on irregularly located points. Therefore, we have removed outliers as described by Stolk et al. (2013). The initial data set (residual Moho) has been interpolated on a $5' \times 5'$ grid. This field has been slightly filtered with a Gauss-type function having the boundary wavelength (half amplitude) 75 km. Points that differ by more than 1.35 km (RMS of the total difference) have been removed from consideration. After interpolation of the remaining points, the initial isostatic correction is restored to obtain the final map (Figure 7).

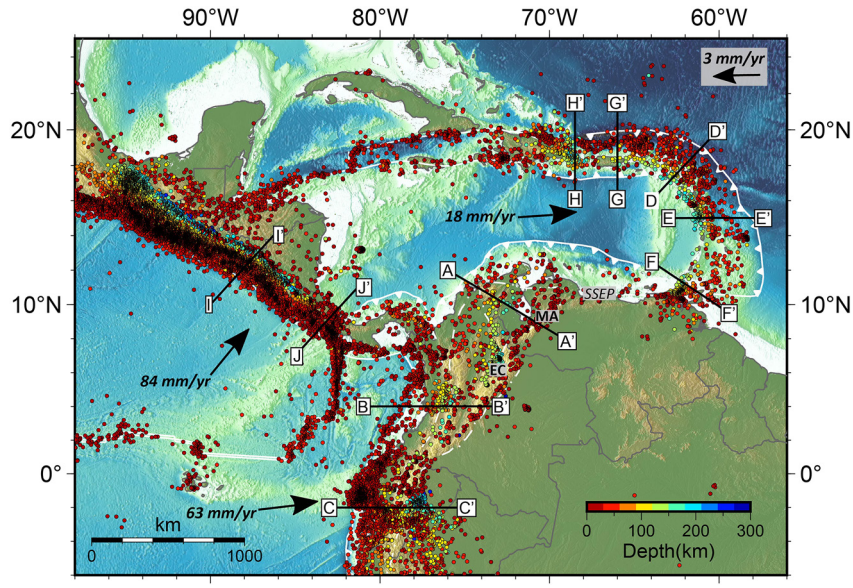

Figure 8. Seismicity of the Caribbean and northern South America region for events $M \geq 4$ between 1 January 2005 and 30 April 2019. Hypocenters are projected onto the cross section from within 50 km. Black arrows denote plate motion rates and directions relative to the South American plate (Argus et al., 2011). Abbreviations: EC—Eastern Cordillera, MA—Merida Andes, and SSEP—San Sebastian-El Pilar fault system.

The crustal thickness map (Figure 7) is consistent with both seismically determined Moho depths and the surface load in the areas without seismic coverage. In general terms, this map shows thicker crust (>25 km) beneath the onshore areas and a thinner crust (5–10 km) in the normal ocean domains. In addition, there are several notable features in the crustal thickness map. Although an oceanic crust with normal thickness was anticipated in the Venezuela basin beneath the area with high positive Bouguer anomaly (Figure 3a; also shown in Diebold et al., 1999), the crustal thickness map shows a wider area that extends from this basin to the eastern side of the Colombia basin through the Aruba gap (AG in Figure 7). Moreover, there are two additional areas of normal-thickness ocean crust: one between the Beata ridge and the SNR and another between the SNR and northern Panama (Figure 7). All these regions with normal oceanic crust are significant because they are within the Caribbean plate, interpreted by some previous studies as an oceanic plateau with a thick (20–25 km) crust (Burke et al., 1978; Kerr et al., 2003).

4.4. Seismicity

The seismicity in the Caribbean region and South America is predominantly shallower than 70 km and is concentrated at plate boundaries and major faults (Figure 8). Shallow events away from the active plate boundaries can be found in the Atlantic Ocean, the Galapagos hot spot, and at the southern tip of the Pedro Bank fault zone (PBFZ, the boundary between the NNR and SNR; Figure 3a). At subduction zones, the events only reach depths of 200 km at the Lesser Antilles and 254 km at Central and northern South America. The deepest events are at 423 and 445 km beneath western South America. All of these depths are less than the maximum depth of 660 km found at some circum-Pacific subduction zones (Hayes et al., 2018). We further analyze the seismicity of Figure 8 in 2D cross sections with four subregions: (a) northern South America, (b) Lesser Antilles, (c) Puerto Rico and Muertos trenches, and (d) Middle American trench (MAT).

4.4.1. Northern and Northwestern South America

Shallow (<50 km) seismicity in northern and northwestern South America, similar to the entire region, is predominantly at plate boundaries: the transform faults between the Cocos and Nazca plate as well as the subduction of the Nazca plate beneath South America (Figure 9a). However, there is a trend of superficial seismicity along the Guaicaramo fault system, at the eastern side of the Eastern Cordillera in Colombia, through the Merida Andes in Venezuela, terminating at the SSEP fault system (Figure 8). Cross-section A–A′ depicts the seismicity

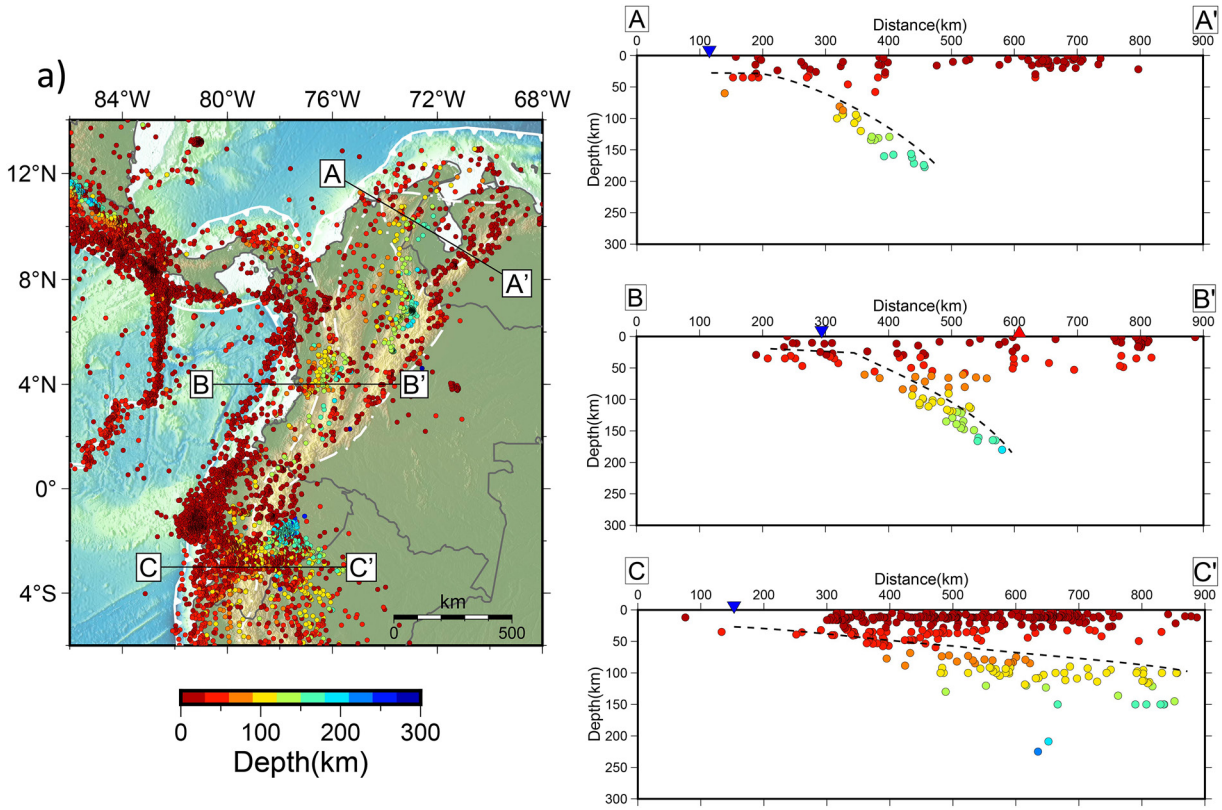

Figure 9. (a) Seismicity of the NW South America (SA) plate and SE Central America for events $M \geq 4$ from 1 January 2005 and 30 April 2019. Cross-section A–A′, looking NE beneath the South Caribbean Deformed Belt. Cross-section B–B′, looking north beneath the northern segment of the Nazca plate subducting beneath the SA plate. Cross-section C–C′, looking north beneath the flat-slab subduction of the Nazca plate beneath the SA plate, south of the Carnegie ridge. Inverted blue triangles show the position of the trench over the cross section and red triangles indicate active volcanoes (Global Volcanism Program, 2013).

across the plate boundary between the Caribbean and South America plates. Although there is no seismic activity at the trench, the hypocenters exist to the southeast and a Benioff zone can be traced to a depth of 175 km. This confirms, as reported in previous papers (Bernal-Olaya et al., 2015; Cornthwaite et al., 2021; Mora et al., 2017; M. Sun et al., 2022; van Benthem et al., 2013), the subduction of the Caribbean plate beneath northern South America and implies that part of the plate has been consumed at this active margin.

The geometry of the subducting Nazca plate varies greatly along the axis of the trench. At 4°N (Cross-section B–B′), the Benioff zone has a steadily increasing dip reaching a depth of 200 km below where volcanism occurs (300 km from the trench). There appear to be earthquakes in the mantle wedge above the slab. It is possible that these events are due to fluid ascent beneath the volcanic arc. A slab depth of 200 km beneath an active volcano is significantly deeper than the average slab depth of 100 km below volcanoes worldwide (Syracuse & Abers, 2006). The Nazca plate beneath central Ecuador (Cross-section C–C′) maintains a gentle dip reaching a depth of 150 km at about 700 km from the trench, and volcanism is absent at this latitude.

4.4.2. Lesser Antilles

Seismicity of the Lesser Antilles is more abundant north of 14°N (Figure 10a). A remarkable feature of the region is the arcuate shape of the plate boundary, which rotates from west-dipping at 12°N to south-dipping at 20°N. The northeastern side of Venezuela has high seismicity that is spread around the SSEP fault system (Figure 10a).

The active subduction of the oceanic lithosphere of the equatorial Atlantic (hereafter referred as the Atlantic slab) beneath the Antilles is clearly visible in the seismicity of the northern and middle Antilles (Cross-sections D–D′ and E–E′, respectively). The subduction geometry at the northeastern corner of the Antilles arc is evident in Cross-section D–D′. The oceanic lithosphere has a gentle dip that increases substantially, with hypocenters reaching depths of 200 km about 300 km from the trench. The Benioff zone is around a depth of 120 km below

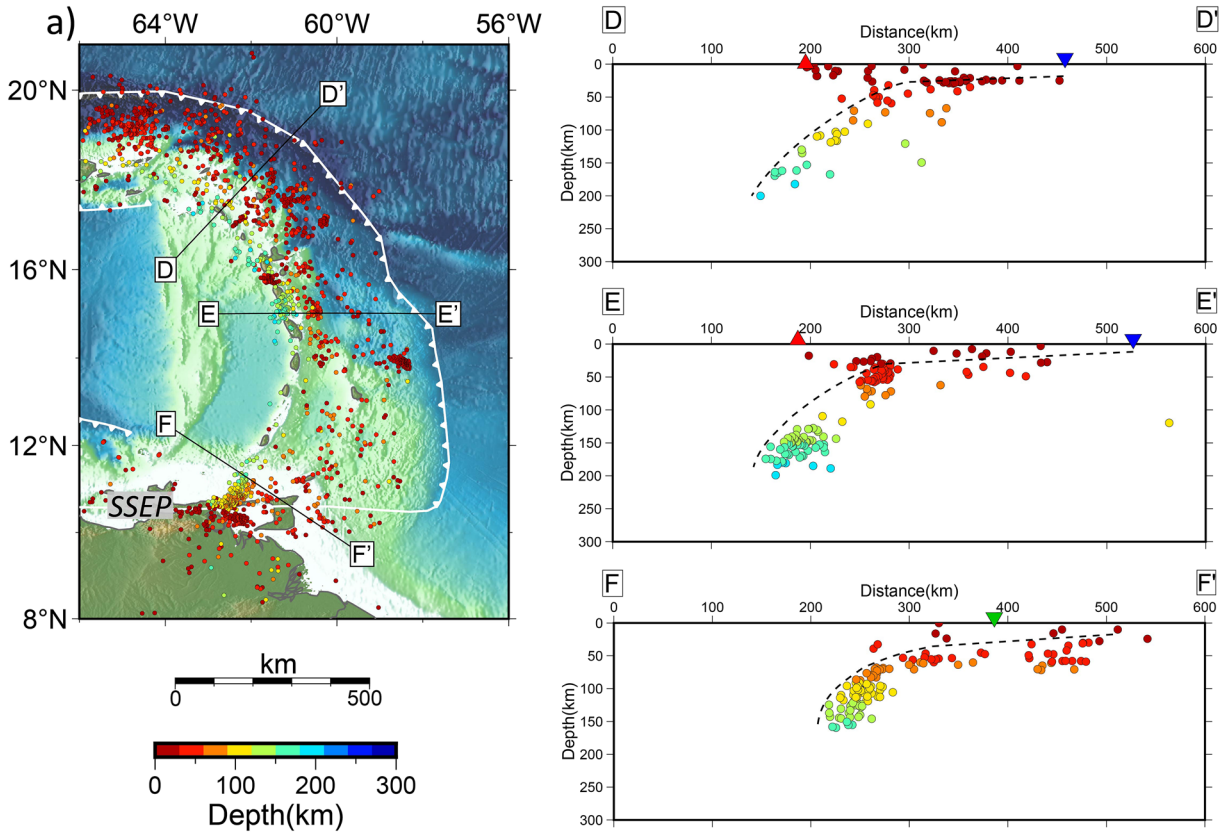

Figure 10. (a) Seismicity of the Lesser Antilles for events $M \geq 4$ from 1 January 2005 and 30 April 2019. Cross-section D–D′, looking north beneath northern segment of the Lesser Antilles Volcanic arc (LAVA), Cross-section E–E′, looking north beneath the middle of the LAVA, and Cross-section F–F′, looking north beneath Trinidad and Tobago (northeast of Venezuela). Inverted triangles show the position of the trench (blue) and transform fault (green) over the cross section. Red triangles are the position of the volcanoes (Global Volcanism Program, 2013). These cross sections clearly define the geometry of the subducting oceanic lithosphere and demonstrate that the seismicity terminates at a depth of 160–200 km depth. Key to abbreviations: SSEP—San Sebastián-El Pilar fault system.

an active volcanic arc (Cross-section D–D′). In contrast, in the central Lesser Antilles arc (Cross-section E–E′), the subducting plate maintains a gentle dip to a distance of 250 km from the trench, and hypocenters deeper than 125 km exist more than 300 km from the trench.

Unexpectedly, in northeastern Venezuela (Cross-section F–F′), there is a Benioff zone despite the fact that the predominant fault in the area is the dextral strike-slip SSEP fault, not an active subduction zone. Rodriguez-Millan (2014) suggests that the current location of the subduction zone beneath the Antilles is at Trinidad and Tobago. However, this location is not consistent with the shallow seismicity that can be seen E-SE of Cross-Section F–F′. Pindell and Kennan (2009) proposed that the subduction zone beneath the Lesser Antilles was located at Trinidad and Tobago during the Miocene (13 Ma), which suggests that the seismicity found in this region is related to that ancient location of the trench, which later migrated to the SE of Trinidad and Tobago (the eastern side of Cross-Section F–F′).

4.4.3. Greater Antilles (Dominican Republic and Puerto Rico Segments)

A microplate with a high level of seismicity is sandwiched between the obliquely subducting North American and Caribbean plates at 64°–72°W (Figure 11a; Clinton et al., 2006). Shallow seismicity is abundant primarily over the Puerto Rico trench and over the Septentrional fault system with intermediate seismicity beneath SW Dominican Republic and some beneath Puerto Rico (Figure 11a). The Muertos trough is a clear bathymetric feature but shallow seismicity is sparse in the vicinity of the trench (Figure 11a).

Cross-section G–G′ indicates that the Atlantic slab subducts obliquely southward beneath Puerto Rico and shows no seismicity associated with northward subduction of the Caribbean plate in Cross-section G–G′ at the Muertos trough, just some shallow events several kilometers to the north. There is a great abundance of intermediate

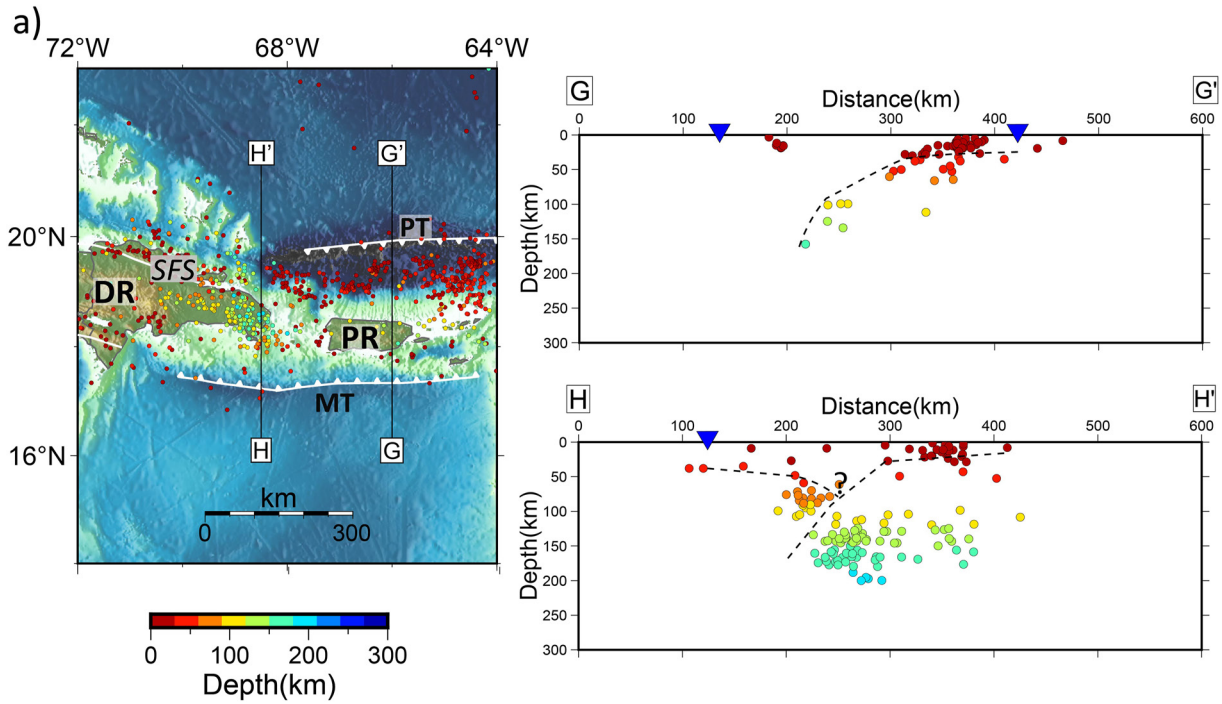

Figure 11. (a) Seismicity of Dominican Republic and Puerto Rico for events $M \geq 4$ from 1 January 2005–30 April 2019. Cross-section G–G′, looking west beneath Puerto Rico (PR) and Cross-section H–H′, looking west beneath Dominican Republic (DR). Blue triangles mark the position of the trench; red triangles indicate volcanoes. Key to abbreviations: PT—Puerto Rico trench, MT—Muertos Trough, and SFS—Septentrional fault system.

depth seismicity at 68.5°W with reduced shallow seismicity (Cross-section H–H′). Following Dolan et al. (1998) and recent gravity modeling from L. Sun et al. (2021), we interpret a collision between the obliquely subducting Atlantic slab and the northward subducted Caribbean plate, leading to a high level of seismicity at depths between 60 and 120 km (Cross-section H–H′).

4.4.4. Middle American Trench

Seismicity is abundant at the MAT (Figure 12a) with the subduction of the Cocos plate beneath the Caribbean plate (Figure 8). Cross-section I–I′ highlights the high seismic activity above 70 km in Middle America, both in the subducting slab and the overriding plate, indicating weak plate coupling. Seismicity can be traced to a depth of 240 km, below which the slab is aseismic. The slab is at a depth of 125 km beneath the active volcanic arc.

Seismicity is abruptly reduced at 82.2°W where the Cocos ridge meets the trench. A consequence of ridge subduction is the restriction of the seismicity to depths shallower than 60 km as seen in seismicity Cross-section J–J′.

A clear Wadati-Benioff zone is evident northwest of the 82.5°W with its associated volcanic arc (Cross-section I–I′). In contrast, the hypocenters that are deeper than 30 km in Cross-section J–J′ display only limited deepening, reaching just 60 km depth. Seismicity south of the trench suggests that the ridge-trench collision causes internal deformation to the Cocos ridge and that because of its buoyancy, the crust cannot reach depths greater than 60 km. This tectonic effect as well as the shallowing of the trench and the partial cessation of volcanic arc activity (Figure 1) are shared characteristics of aseismic ridges at subduction zones worldwide (Adamek et al., 1987; Kelleher & McCann, 1976; Vogt et al., 1976).

4.5. P-Wave Tomography Model

The deep lithospheric and mantle structure of South America and the Caribbean has been investigated using seismic tomography (Bijwaard et al., 1998; Braszus et al., 2021; Celli et al., 2020; Cornthwaite et al., 2021; Obayashi et al., 2013; Sallarès et al., 2000; Schaeffer & Lebedev, 2013; Simmons et al., 2012; M. Sun et al., 2022; van Benthem et al., 2013; Zhu et al., 2020). A recent teleseismic P-wave tomography model (DETOX-P1) has brought the geometries of subducted slabs under South America into sharper focus through the use of regional

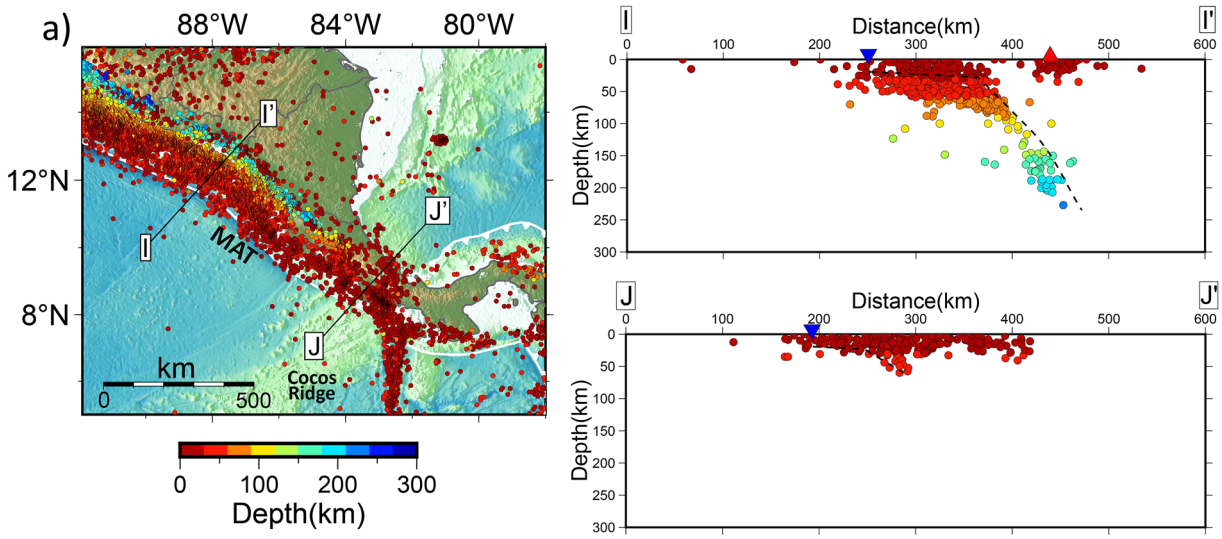

Figure 12. (a) Seismicity of the Middle American Trench (MAT) for events $M \geq 4$ between 1 January 2005 and 30 April 2019. Cross-section I–I′, looking northwest beneath the MAT. Cross-section J–J′, looking northwest beneath the collision of the Cocos ridge with the MAT. Blue triangles mark the position of the trench; red triangles indicate volcanoes.

South American data (Hosseini et al., 2020; Mohammadzaheri et al., 2021). We have extracted three unpublished sections to obtain images of the geometry and extent of the subducting slabs in our study area (Figure 13).

Cross-section A–A′ is oriented NW-SE and extends from the Yucatan platform to central Brazil (Figure 13). An image of the Caribbean slab (CA) that has subducted beneath NW South America is evident in Cross-section A–A′. The tomographic image shows that the Caribbean slab is present to depths of at least 660 km and may reach another high-velocity anomaly at a depth of 800–1,200 km. Results from a well-resolved finite-frequency tomography velocity model of Colombia and western Venezuela (M. Sun et al., 2022) agree with the great depth (around 660 km) to which the Caribbean plate can be seen, but given their limited resolution at greater depths, M. Sun et al. (2022) do not discuss the deeper anomaly we observe. We interpreted this deeper anomaly as a possible relic of the Farallon plate that was connected to the Caribbean plate before 100 Ma as recent paleomagnetic studies have suggested (Boschman et al., 2019). The mantle beneath the western Caribbean has low P-wave velocities in the upper mantle, mantle transition zone, and locally to a depth of 900 km, whereas the mantle of northern South America has a near-zero anomaly. We discuss the low P-wave velocities below.

Cross-section B–B′ is oriented E-W from the Cocos plate through the Caribbean to the Atlantic Ocean (Figure 13). This cross-section images the Cocos slab (CO) subducting at the MAT and reaching a depth of at least 1,800 km. The slab is deflected horizontally at the 410 km discontinuity but passes through the 660 km discontinuity unhindered. The Atlantic slab is clearly imaged and reaches depths greater than 660 km beneath the Lesser Antilles. The upper mantle beneath the Caribbean displays strong lateral variations in P-wave velocity, ranging from strongly negative in the west to a near-zero velocity anomaly to the east beneath the Venezuela basin (66°–70°W).

Cross-section C–C′ is oriented NE-SW and extends from the Cocos plate across the Nicaraguan rise and Hispaniola to the Atlantic Ocean (Figure 13). This cross-section clearly images the subduction of the Cocos slab at the MAT. The slab subducts steeply, is not deflected at either the 410 or 660 km discontinuities, and is visible to a depth of at least 1,800 km. Beneath the Caribbean, the upper mantle, mantle transition zone, and lower mantle to a depth of 1,000 km show pronounced low P-wave velocity anomalies, consistent with Cross-sections A–A′ and B–B′. In contrast, the upper mantle beneath the Atlantic Ocean with age 120 Ma has a near-zero seismic anomaly.

Cross-sections A–A′ and C–C′ from the DETOX-P1 tomography model (Figure 13) are coincident with P-wave cross sections from the model UU-P07 presented by van Benthem et al. (2013). There is excellent agreement between these tomographic models. DETOX-P1 Cross-section A–A′ (Figure 13a) and model UU-P07 are unambiguous in confirming the subduction of the high-velocity Caribbean slab to the mantle transition zone. However, in model UU-P07, the Caribbean slab flattens at the 660-discontinuity, whereas this flattening is not evident in the DETOX-P1 model (Figure 13a). The positions of the Cocos and Farallon slabs (Figure 13a) are highly

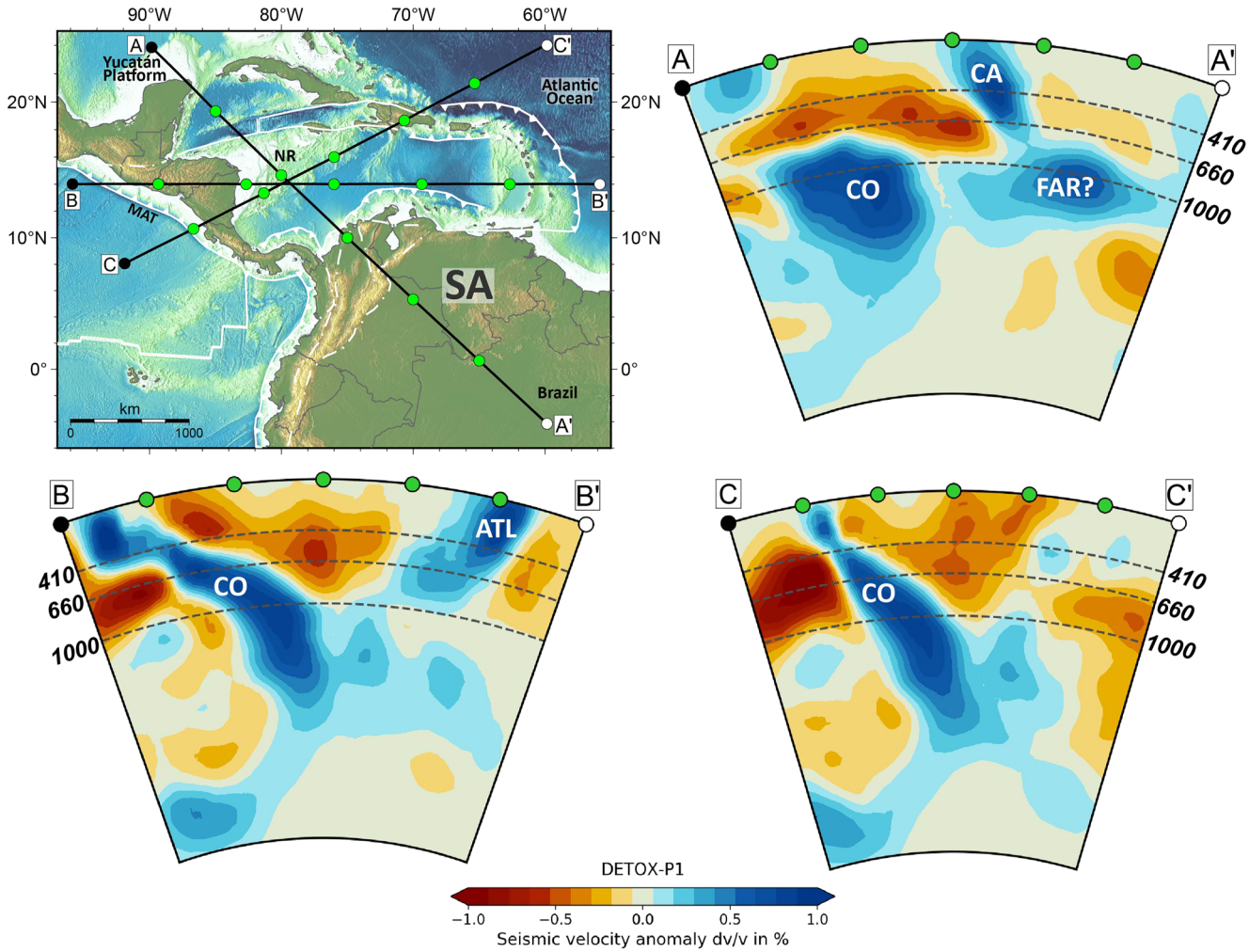

Figure 13. Vertical sections of the tomography model DETOX-P1 (Hosseini et al., 2020; Mohammadzaheri et al., 2021) through Cross-section A–A′, Yucatan platform, Nicaraguan rise, NW South America, and Brazil. Cross-section B–B′, Middle American Trench (MAT), central Caribbean, and the Lesser Antilles subduction zone. Cross-section C–C′, MAT, Southern Nicaraguan Rise (SNR), Dominican Republic, and the Atlantic Ocean. Dashed lines mark 410, 660, and 1,000 km depth. Seismically faster-than-average P wave anomalies are shown in blue shades, slower-than-average anomalies are shown in red. Labels in the sections: CA: Caribbean slab, CO: Cocos slab, FAR: Farallon slab, ATL: Atlantic slab.

consistent in the DETOX-P1 and UU-P07 models. Cross-section C–C′ from DETOX-P1 depicts the Cocos slab subducted through the mantle transition zone and extending into the lower mantle. This deep subduction agrees with the UU-P07 model. Beneath the Caribbean plate, the DETOX-P1 and UU-P07 models both consistently show low P-wave anomalies that are bounded by high-velocity subducting slabs (Figure 14).

A comparison of the DETOX-P1 tomography model (Hosseini et al., 2020; Mohammadzaheri et al., 2021) with the recent S-wave tomographic models of Zhu et al. (2020) and Celli et al. (2020) shows: (a) excellent agreement for the geometry and depth extent of the high-velocity subducting slabs and (b) poor agreement for the strength of the low-velocity features beneath the Caribbean plate.

5. Discussion

5.1. Central America, Colombia, and Eastern Pacific

A strong magnetic anomaly with a high-to-low signal is found beneath southern Costa Rica, Panama, and northwestern Colombia (Figure 14a). We infer that this anomaly is related to the Panama-Choco block (PCB; Figure 14a), a block that is colliding with the northwestern margin of the South American plate since middle

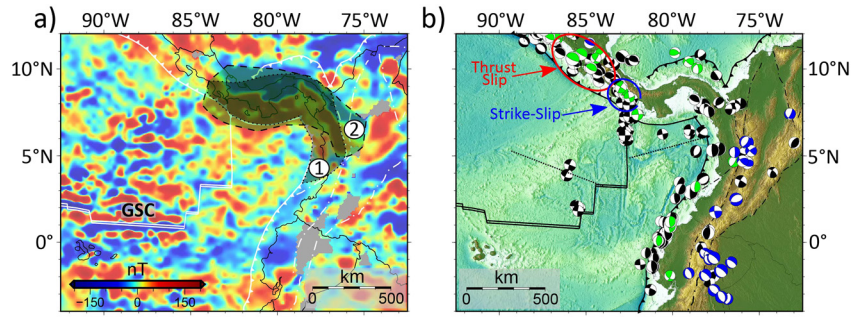

Figure 14. (a) Magnetic anomaly map from EMAG2v3 (Meyer et al., 2017) over southern Costa Rica, Panama, and northwestern Colombia. There is a strong high-to-low magnetic anomaly related to the collision of the Panama-Choco block (PCB) with the northwestern margin of the South American plate. Block 1 is the PCB as interpreted by previous authors (Mora-Páez et al., 2019), whereas block 2 is our interpretation as defined by the magnetic anomaly. The interpretation of block 2 agrees with the Panama indenter model of Vargas and Mann (2013), which hypothesizes that an extinct island arc is being subducted beneath northwestern South America. Key to abbreviation: GSC Galapagos Spreading Center. (b) Focal mechanisms from the Global Centroid Moment Tensor Catalog (Ekström et al., 2012); color according to hypocentral depth: black (<30 km), green (30–100 km), and blue (>100 km). At the northeastern side of the Cocos ridge, the primary component of the focal mechanisms is of thrust slip. Where the Cocos ridge is in contact with the Middle American Trench (MAT), the focal mechanisms have mainly a strike-slip component. Thin dashed lines are suture zones with a left-lateral component that indicate deformation within the Cocos ridge and the northern segment of the Nazca plate.

Miocene times and is responsible for the closing of the Central American seaway (Montes et al., 2015, 2019; Wagner et al., 2017).

The high-to-low magnetic anomaly correlates very well in Costa Rica and Panama with the PCB interpreted by previous authors (Camacho et al., 2010; Montes et al., 2015, 2019; Mora-Páez et al., 2019; Wagner et al., 2017, Figure 14a, block 1); however, in NE Colombia, the anomaly looks shifted toward the northeast (Figure 14a, block 2). This block 2 agrees with the position of the southern border of the Panama indenter model of Vargas and Mann (2013), which is related to the Caldas Tear around 5°N and the variation from a southern steep downdip to a northern shallow downdip of the subducting slab (Vargas & Mann, 2013). Moreover, an analysis of the volcanic patterns over the past 14 Ma in this region suggests that despite there is an offset of the volcanic arc at the Caldas Tear, it was continuous from 1.5° to 7°N by 12 Ma (before the collision of the PCB and crossing the Caldas Tear; Wagner et al., 2017). This indicates that this offset occurs in the same subducting Nazca plate and is not a boundary between two plates (Wagner et al., 2017) and agrees with our interpretation of the continuous positive P-wave anomaly from the depth sections shown by Mohammadzaheri et al. (2021).

At the western end of the PCB, focal mechanisms provide further evidence for the effects of the Cocos ridge on subduction of the Cocos plate beneath the MAT. Most focal mechanisms on the western side of the colliding ridge have a thrust component. In contrast, where the Cocos ridge is in contact with the MAT and to the east, the motion of most focal mechanisms turns to a dextral strike slip (Figure 14b). We infer that the buoyancy of the ridge hinders normal subduction of the Cocos plate at the MAT, resulting in a realignment of the stress regime as evidenced by the change in focal mechanisms. Models of continental indentation predict that the shallow subduction of the Cocos ridge may generate subhorizontal compressive stresses parallel to the axis of the rigid indenter (ridge), which cause indentation along trench-perpendicular strike-slip faults (Kolarsky et al., 1995).

5.2. Interaction Between Continental Blocks, Great Arc of the Caribbean, and Caribbean Large Igneous Province

The collision of the Cuban segment of the GAC with the Bahama platform in the Paleocene to middle Eocene is hypothesized to have resulted in the shift in the motion of the Caribbean plate from a northeastward direction to an eastward direction (Carvajal-Arenas & Mann, 2018). This shift in turn led to the initiation of two basins: the YB and the CT (Figure 15).

In the magnetic anomaly map, only the Cayman ridge can be differentiated by its positive magnetic anomaly. This positive anomaly is surrounded by a negative magnetic anomaly that underlies most of the YB and is continuous

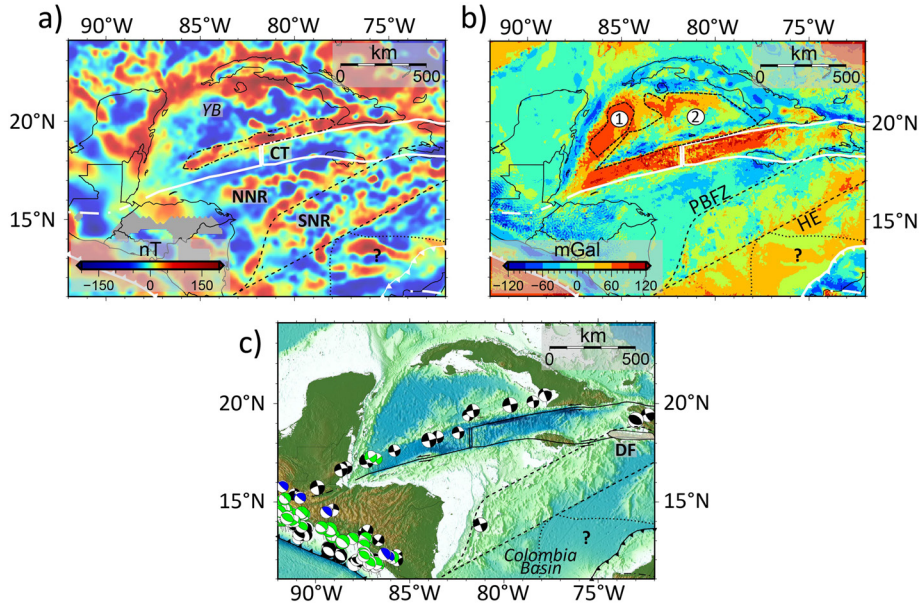

Figure 15. (a) Magnetic anomaly map from EMAG2v3 (Meyer et al., 2017). The bounded area with a dotted-dashed line represents the positive magnetic anomaly generated by the Cayman ridge (between the Yucatan basin—YB and the Cayman trough—CT). (b) Residual gravity anomaly map with basement domains defined by Rosencrantz (1990): 1. Western deep basin and 2. Eastern basin, Cayman Rise, Cayman Ridge, and Camagüey trench (mentioned from north to south and west to east). (c) Focal mechanisms from the Global Centroid Moment Tensor Catalog (Ekström et al., 2012). Color of the focal mechanisms according to depth: black (<30 km), green (30–100 km), and blue (>100 km). Thin dashed lines indicate the interpreted location of the Pedro Bank Fault Zone (PBFZ) and the Hess Escarpment (HE), structures that interact at the northwest with the Duarte Formation (DF) through the Enriquillo fault (Leroy et al., 2000). Area bounded by a dotted line and with a question mark represents a segment of oceanic crust within the Colombia basin with different magnetic and residual anomalies as well as different bathymetry from the rest of the basin. When investigating further the crustal structure from the sources in the database, we found a normal oceanic crust thickness (8 km).

toward the CT (Figure 15a). The residual gravity anomalies of the YB correlate with two crustal types defined by Rosencrantz (1990) based on seismic reflection data. Crustal-type one is Eocene oceanic crust with positive residual anomalies ranging between 60 and 90 mGal (Figure 15b, basement 1). Crustal-type two is a pre-Paleogene oceanic basement covered by a sequence of volcanic and plutonic rocks/features, like the Cayman Rise, Cayman ridge, and the eastern basin (Figure 15b, basement number 2; See more in Rosencrantz, 1990). The Cayman Rise and Cayman ridge are characterized by negative residual anomalies (the lowest of which is found along the Cayman ridge), whereas positive anomalies are found beneath the eastern basin.

In general, we can observe a correlation between negative magnetic anomalies, positive residual gravity anomalies, and deep bathymetry features (Figure 15b). The YB and the eastern basin, together with the CT, share these physical characteristics. In agreement with Leroy et al. (2000), we infer this is because the YB and eastern basin formed the northwestern margin of the Caribbean plate under a trans-tensive regime until the Eocene. The GAC then collided with the Bahamas platform and modified the regional stresses into a more east-west trend. This in turn promoted the formation of the CT.

The Nicaraguan Rise is divided into a northern (NNR) and southern (SNR) domain by the PBFZ as clearly defined by the residual gravity anomaly map (Figure 15b). We note that Cretaceous rocks are reported for both domains (Carvajal-Arenas et al., 2020). The NNR, which has been interpreted as a thinned continental crust and the extension of the continental Chortis block (Boschman et al., 2014; Donnelly, 1994), has negative residual gravity anomalies (0 to −60 mGal) extending from offshore Nicaragua and Honduras to Jamaica. In the case of the SNR, the residual gravity anomaly is more irregular and ranges from negative to positive values (from −60 to 60 mGal) and is interpreted as part of the CLIP (Boschman et al., 2014). Moreover, a continuation of the seismic reflector that has been described as the top of the plateau basalt of the Caribbean plate (also known as B″ Horizon) was found at site 152 of the Deep-Sea Drilling Project, which is situated over the SNR (Donnelly, 1994).

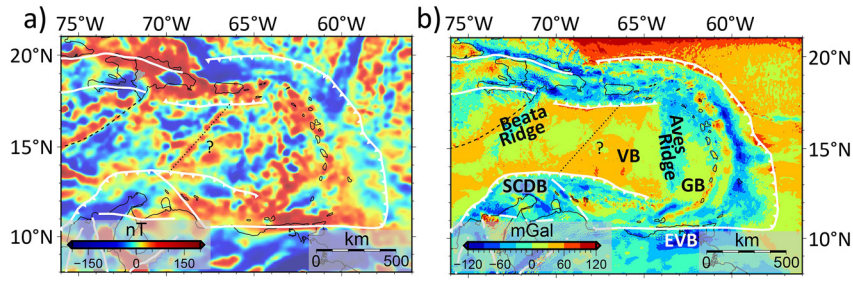

Figure 16. (a) Magnetic anomaly map from EMAG2v3 (Meyer et al., 2017). Dashed line at the western side of the Beata Ridge is the interpreted location of the Hess Escarpment. (b) Residual gravity anomaly map. Dotted line with a question mark is the place where the NE-SW magnetic lineament stops. Key to new abbreviations: GB—Grenada basin, EVB—Eastern Venezuela Basin.

The segmentation of the Nicaraguan Rise and its tectonic setting was also corroborated by the magnetic anomaly map (Figure 15a) and the focal mechanisms (Figure 15c). Even though the magnetic anomalies beneath NNR and SNR both have a NE-SW trend, we observe that the magnetic anomalies at NNR are broader than the ones at SNR (Figure 15a). We also observed that the left-lateral strike slip mechanism found in the SNR (Figure 15c) agrees with the proposal that there exists a transtensional regime in the SNR (Carvajal-Arenas & Mann, 2018). This regime is generated by the northeastward motion of the SNR, which also led to a compression regime at southwestern Hispaniola (along the Enriquillo-Plantain Garden Fault; Carvajal-Arenas & Mann, 2018). This was also corroborated by the thrust and sinistral focal mechanisms north of the Dumisseau formation (Figure 15c).

5.3. Regions With Normal-Thickness Ocean Crust Within the Caribbean Plate

Overall, the magnetic and residual anomalies within the Caribbean plate do not have a clear trend. García-Reyes and Dyment (2021) suggest the absence of the typical lineated seafloor spreading anomalies is because the plate was probably formed during the Cretaceous Normal Superchron; however, they and other authors have been able to identify some anomalies within the Colombia and Venezuela basins (Christofferson, 1973; García-Reyes & Dyment, 2021). Our geophysical data also allowed us to interpret some of these trends as well as a relationship with the crustal thickness. We observed a segment with the W-E linear magnetic anomalies found by Christofferson (1973) in the Colombia basin (bounded by dashed lines in Figure 15a). Moreover, we found a correlation of the magnetic anomalies with residual anomalies lineaments (Figure 15b) and a segment of normal-thickness ocean crust (Figure 7). Furthermore, the topography within the segment is smoother and deeper than the rest of the Colombia basin (Figure 15c).

A NE-SW magnetic lineament can be interpreted at the western side of the Venezuela basin (VB in Figure 16a). This is consistent with the results of García-Reyes and Dyment (2021), who relate these lineaments to a major fault zone (García-Reyes & Dyment, 2021). In addition, we found the magnetic lineament coincides with the boundary of a region with normal-thickness (7 km) oceanic crust at the eastern side of the basin (Figure 7) and a trend of a higher residual anomaly (30–60 mGal) that interrupts a lower one (0–30 mGal; dashed line in Figure 16b). This marks a limit or transition to a region with normal-thickness oceanic crust in the SE of the Venezuela basin.

The region with a normal-thickness ocean crust segment in the Venezuela basin was interpreted as a back-arc basin related to the Aves ridge remnant arc by previous studies (Aitken et al., 2011; Allen et al., 2019; Romito & Mann, 2020). However, the oceanic crust segment we interpreted is at least five times larger than the Grenada basin, the back-arc basin related to the eastward migration of the arc volcanism from the Aves ridge to the Lesser Antilles. Furthermore, the size and shape of the normal ocean crust segment within the Caribbean plate that we interpreted in the crustal thickness map (Figure 7) is even more wide and complex and the tomography section does not show any slow P wave velocity anomaly that suggests partial melting. We instead suggest that the ocean crust of the Venezuela basin formed in the Pacific during the Jurassic-Cretaceous as suggested by Mauffret and Leroy (1997), and also proposed based on an analysis of marine magnetic data (García-Reyes & Dyment, 2021). Deformation of the southern tip of the Aves ridge, the Lesser Antilles and the Leeward Antilles (Figure 16b; GAC; Kroehler et al., 2011; Vence & Mann, 2020) and portions of the oceanic plateau in the offshore of Venezuela

(Figure 4b) provide evidence of the ongoing eastward movement of the Caribbean plate, and the southern boundary of the block moving to the east. Also, a slab tear or STEP fault (subduction transform edge propagator, Govers & Wortel, 2005) as indicated by Mora et al. (2017) would be present where the SSEP dextral strike-slip fault (Figure 8) and the convergent boundary meet, indicating the SW corner of the Caribbean plate.

5.4. Maximum Earthquake Depths and the Geometry of Subducted Slabs

Hayes et al. (2018) investigated the geometry of subducted slabs on a global basis and identified the seismicity of the Antilles and Central American subduction zones as extending to a depth of 200 km, whereas seismicity reaches 660 km beneath much of South America, the SW Pacific, and Japan. Syracuse et al. (2010) present a range of two-dimensional subduction zone thermal models showing that older slabs have a much colder thermal structure that is consistent with deeper (660 km) seismicity as the brittle-ductile transition persists to a greater depth. Seismic tomography models (Mohammadzaheri et al., 2021) show that the subducting slabs in the circum-Caribbean extend into the lower mantle, below the bottom of the mantle transition zone at 660 km depth. However, as shown in Figure 17, seismicity does not reach depths greater than 200 km, whereas the tomography Cross-sections A–A′, B–B′, and D–D′ display that the slabs go deeper than this.

The relationship between the maximum depth of slab seismicity and the physical state of the slab is discussed by Kirby et al. (1996). These authors introduced the concept of the slab thermal parameters, defined as the age of the slab where it subducts times the convergence rate. The intuitive concept is that old and cold slabs with high convergence rate will have deeper earthquakes than a young and warm slab with a low convergence rate. The work of Kirby et al. (1996) was revisited by Syracuse et al. (2010) who present a global compilation that confirms the utility of the thermal parameter. Our calculations of the thermal parameter (Table S1 in Supporting Information S1) for the MAT and the Greater Antilles are consistent with the global group of slabs that do not have seismicity below 200 km depth.

6. Conclusions

The analysis of multiple geophysical data sets provides new and improved images of the crust and mantle of the Caribbean, northern South America, and their tectonically active boundaries. We focus on the geophysical definition of the terranes that constitute the Caribbean and northern South America and that are important to the tectonic evolution of the region. We investigate the physical properties and thickness of the crust with a residual gravity anomaly map, a new crustal thickness map, and a magnetic map. We also examine the deeper crust and mantle with seismicity cross sections and a recent P-wave mantle tomography model.

At the Pacific plate boundary, focal mechanisms revealed that the Cocos and Malpelo ridges are undergoing internal deformation and are modifying the plate boundaries between the Caribbean, Cocos, and Nazca plates (Figure 13). In a similar way, we find that the collision of the PCB with northwestern South America has also deformed the Nazca, South American, and Caribbean plate boundaries as well as the shallow slab geometry and seismicity of the subducting Nazca and Caribbean slabs. Moreover, at the eastern side of the Caribbean plate, there is evidence for the deformation of the southern tip of the Aves ridge and the Lesser Antilles. This is the surface consequence of the collision with the northwestern margin of the South American plate that left remnants of the former GAC and/or CLIP (Figure 16b).

Seismicity at widely separated circum-Caribbean subduction zones rarely exceeds 200 km in depth, whereas the actively subducting slabs reach the bottom of the mantle transition zone or deeper (Figure 17). We hypothesize that the thermal structures of these subduction zones are similar (Syracuse et al., 2010), leading to comparable P-T conditions and metamorphic reactions with depth, including dehydration that leads to volcanism (Abers et al., 2013; Hacker et al., 2003). The implication of the observation of deep (>660 km) subduction is that even though seismicity terminates at 200 km depth, subduction has been long-lived at these active margins.

Previous studies of the Caribbean plate have emphasized the role of voluminous plume volcanism that led to the creation of the CLIP (Burke et al., 1978). However, our crustal thickness map (Figure 7), integrated with our interpretations of the simple Bouguer and residual anomaly maps (Figure 3), indicates that large portions of the Venezuela and Colombia basins, which comprise a significant part of the Caribbean plate, are composed of normal-thickness oceanic crust. This is in accord with the findings of Diebold et al. (1999), García-Reyes and

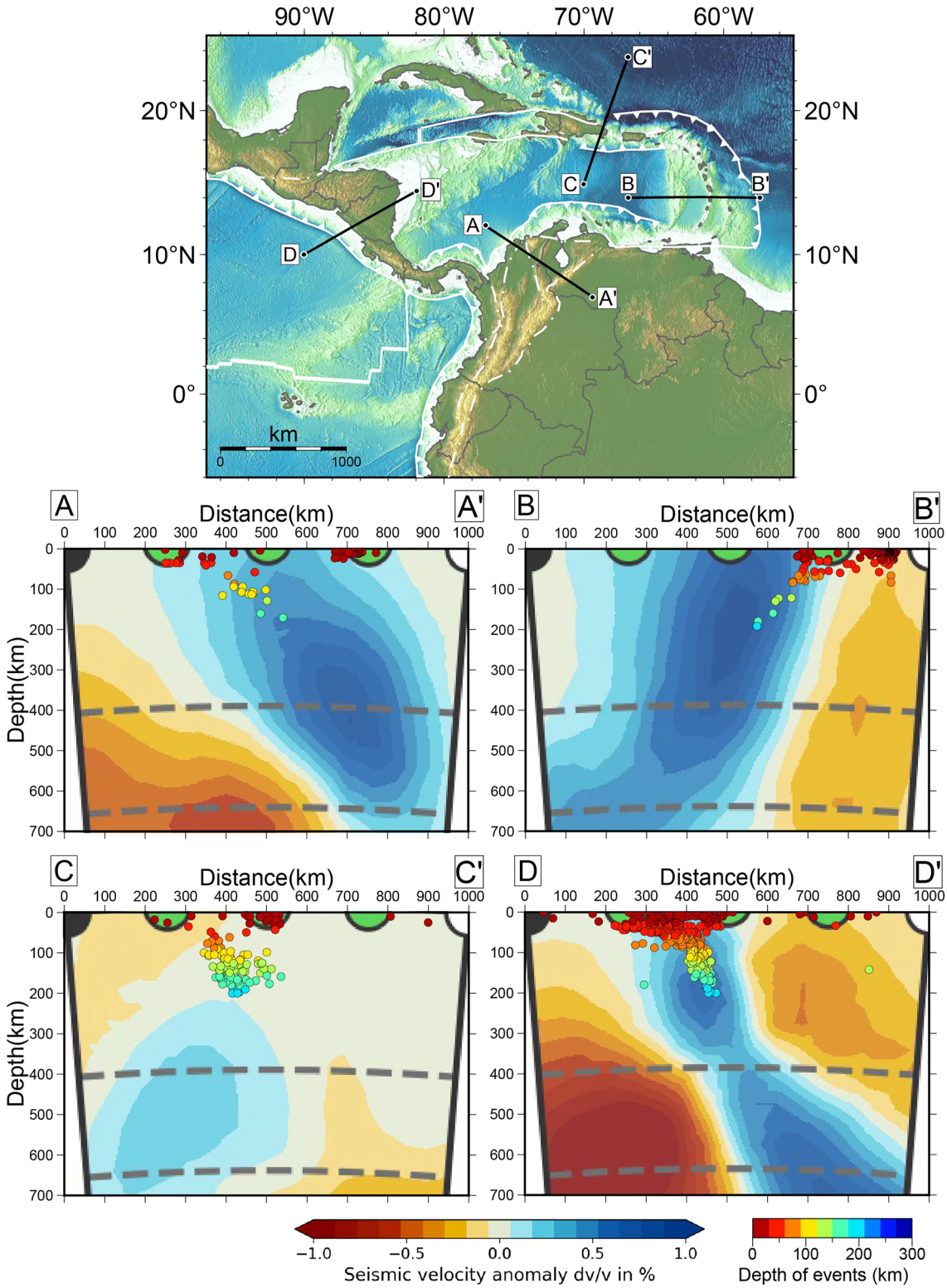

Figure 17. Seismicity overlain on the tomography model DETOX-P1 (Hosseini et al., 2020; Mohammadzaheri et al., 2021). Top: Location map. Bottom: Four cross sections. Cross-section A–A′, NW South America. Cross-section B–B′, the Lesser Antilles subduction zone. Cross-section C–C′, eastern Dominican Republic. Cross-section D–D′, Middle American Trench (MAT). Dashed lines mark the projected depths of 410 and 660 km over the tomography sections.

Dyment (2021), and Romito and Mann (2020). Furthermore, rather than resisting subduction, as expected of thick buoyant crust of an igneous province, seismic tomography images show that the Caribbean plate has subducted to a depth of at least 600 km beneath northern Colombia (Figures 13 and 17; Hosseini et al., 2020; Mohammadzaheri et al., 2021; Schaeffer & Lebedev, 2013; Zhu et al., 2020).

These observations lead us to conclude that a significant portion of the total area of the original Caribbean plate, including the subducted portion, was normal oceanic crust. The present-day Caribbean plate includes regions with normal-thickness crust in the Venezuela and Colombia basins, as well as narrow ridges and plateaus with thickened crust (Figure 7). As proposed in the Pacific origin model (Figure 2), the Caribbean plate likely migrated eastward from the Pacific Ocean as an oceanic plate mostly with normal-thickness crust and limited portions of the crust thickened by hot spot volcanism (CLIP). Furthermore, those portions of the migrating Caribbean plate with thickened crust would cause deformation at the plate boundaries as we can observe in the Pacific plate boundary with the Cocos ridge and the PCB.

Conflict of Interest

The authors declare no conflicts of interest relevant to this study.

Data Availability Statement

The figures in this paper were made with the version 6 of the Generic Mapping Tools software (Wessel et al., 2013). The Supporting Information includes the filtered data points taken from the Global Crustal Database (Mooney, 2015) and the points added as mentioned in the text. This data file and other Supporting Information can be found at Barrera-Lopez et al. (2022) [Data Set].

References

Abers, G. A., Nakajima, J., van Keken, P. E., Kita, S., & Hacker, B. R. (2013). Thermal–petrological controls on the location of earthquakes within subducting plates. *Earth and Planetary Science Letters*, *369*, 178–187. https://doi.org/10.1016/j.epsl.2013.03.022

Adamek, S., Tajima, F., & Wiens, D. A. (1987). Seismic rupture associated with subduction of the Cocos Ridge. *Tectonics*, *6*(6), 757–774. https://doi.org/10.1029/TC006i006p00757

Aitken, T., Mann, P., Escalona, A., & Christeson, G. L. (2011). Evolution of the Grenada and Tobago basins and implications for arc migration. *Marine and Petroleum Geology*, *28*(1), 235–258. https://doi.org/10.1016/j.marpetgeo.2009.10.003

Albuquerque, D. F., França, G. S., Moreira, L. P., Assumpção, M., Bianchi, M., Barros, L. V., et al. (2017). Crustal structure of the Amazonian Craton and adjacent provinces in Brazil. *Journal of South American Earth Sciences*, *79*, 431–442. https://doi.org/10.1016/j.jsames.2017.08.019

Allen, R. W., Collier, J. S., Stewart, A. G., Henstock, T., Goes, S., & Rietbrock, A., & VoiLA Team. (2019). The role of arc migration in the development of the Lesser Antilles: A new tectonic model for the Cenozoic evolution of the eastern Caribbean. *Geology*, *47*(9), 891–895. https://doi.org/10.1130/G46708.1

Argus, D. F., Gordon, R. G., & DeMets, C. (2011). Geologically current motion of 56 plates relative to the no-net-rotation reference frame. *Geochemistry, Geophysics, Geosystems*, *12*(11). https://doi.org/10.1029/2011GC003751

Barrera-Lopez, C., Mooney, W. D., & Kaban, M. K. (2022). Regional geophysics of the Caribbean and northern South America: Implications for tectonics [Data set]. Zenodo. https://doi.org/10.5281/zenodo.6495390

Barthelmes, F. (2009). *Definition of functionals of the geopotential and their calculation from spherical harmonic models: Theory and formulas used by the calculation service of the International Centre for Global Earth Models (ICGEM)*. Retrieved from http://icgem.gfz-potsdam.de

Bernal-Olaya, R., Mann, P., & Vargas, C. A. (2015). Earthquake, tomographic, seismic reflection, and gravity evidence for a shallowly dipping subduction zone beneath the Caribbean Margin of Northwestern Colombia. *AAPG Memoir 108*, 247–269. Retrieved from https://archives.datapages.com/data/specpubs/memoir108/data/247_aapg-sp1970247.htm#purchaseoptions

Bijwaard, H., Spakman, W., & Engdahl, E. R. (1998). Closing the gap between regional and global travel time tomography. *Journal of Geophysical Research*, *103*(B12), 30055–30078. https://doi.org/10.1029/98JB02467

Blakely, R. J. (1995). *Potential theory in gravity and magnetic applications* (p. 441). Cambridge University Press. Retrieved from https://www.google.com/books/edition/Potential_Theory_in_Gravity_and_Magnetic/qGZV-P8bt6gC?hl=en&gbpv=1&pg=PA1&printsec=frontcover

Boschman, L. M., Van der Wiel, E., Flores, K. E., Langereis, C. G., & van Hinsbergen, D. J. (2019). The Caribbean and Farallon plates connected: Constraints from stratigraphy and paleomagnetism of the Nicoya Peninsula, Costa Rica. *Journal of Geophysical Research: Solid Earth*, *124*(7), 6243–6266. https://doi.org/10.1029/2018JB016369

Boschman, L. M., van Hinsbergen, D. J., Torsvik, T. H., Spakman, W., & Pindell, J. L. (2014). Kinematic reconstruction of the Caribbean region since the Early Jurassic. *Earth-Science Reviews*, *138*, 102–136. https://doi.org/10.1016/j.earscirev.2014.08.007

Braszus, B., Goes, S., Allen, R., Rietbrock, A., Collier, J., Harmon, N., et al. (2021). Subduction history of the Caribbean from upper-mantle seismic imaging and plate reconstruction. *Nature Communications*, *12*(1), 1–14. https://doi.org/10.1038/s41467-021-24413-0

Burke, K., Fox, P. J., & Şengör, A. M. C. (1978). Buoyant ocean floor and the evolution of the Caribbean. *Journal of Geophysical Research*, *83*(B8), 3949–3954. https://doi.org/10.1029/JB083iB08p03949

Camacho, E., Hutton, W., & Pacheco, J. F. (2010). A new look at evidence for a Wadati–Benioff zone and active convergence at the north Panama deformed belt. *Bulletin of the Seismological Society of America*, *100*(1), 343–348. https://doi.org/10.1785/0120090204

Canales, J. P., Ito, G., Detrick, R. S., & Sinton, J. (2002). Crustal thickness along the western Galápagos Spreading Center and the compensation of the Galápagos hotspot swell. *Earth and Planetary Science Letters*, *203*(1), 311–327. https://doi.org/10.1016/S0012-821X(02)00843-9

Acknowledgments

The support of the US Geological Survey Earthquake Hazards Program is gratefully acknowledged. The authors also want to thank D. Bird, D. Muñoz-Granados, and R. J. Blakely for their help with the interpretation of the gravity and magnetic anomaly maps as well as the tectonic evolution of the region. In addition, the authors want to thank J. A. Reid, M. G. Cilia, A. R. Blanchette, and M. Hunter for their insightful reviews and comments, and A. K. Shah, A. Mohammadzaheri, and M. Barazangi for technical assistance. Reviews by A. Garcia-Reyes, two anonymous reviewers, and associate editor P. Mann allowed us to clarify and improve this paper.

Carvajal-Arenas, L. C., & Mann, P. (2018). Western Caribbean intraplate deformation: Defining a continuous and active microplate boundary along the San Andres rift and Hess Escarpment fault zone, Colombian Caribbean Sea. *AAPG Bulletin*, *102*(8), 1523–1563. https://doi.org/10.1306/12081717221

Carvajal-Arenas, L. C., Torrado, L., Mann, P., & English, J. (2020). Basin modeling of Late Cretaceous/Mio-Pliocene petroleum system of the deep-water eastern Colombian Basin and South Caribbean Deformed Belt. *Marine and Petroleum Geology*, *121*, 104511. https://doi.org/10.1016/j.marpetgeo.2020.104511

Castillo, K., & Mann, P. (2021). Structure, stratigraphy, and hydrocarbon potential of the easternmost part of the Eastern Venezuelan foreland basin. *Memoir 123: South America—Caribbean—Central Atlantic Plate Boundary: Tectonic Evolution, Basin Architecture, and Petroleum Systems*, 591–620. https://doi.org/10.1306/13692259M123861

Celli, N. L., Lebedev, S., Schaeffer, A. J., Ravenna, M., & Gaina, C. (2020). The upper mantle beneath the South Atlantic Ocean, South America and Africa from waveform tomography with massive data sets. *Geophysical Journal International*, *221*(1), 178–204. https://doi.org/10.1093/gji/ggz574

Christeson, G. L., Mann, P., Escalona, A., & Aitken, T. J. (2008). Crustal structure of the Caribbean–northeastern South America arc-continent collision zone. *Journal of Geophysical Research*, *113*(B8). https://doi.org/10.1029/2007JB005373

Christofferson, E. (1973). Linear magnetic anomalies in the Colombia basin, central Caribbean Sea. *The Geological Society of America Bulletin*, *84*(10), 3217–3230. https://doi.org/10.1130/0016-7606(1973)84%3C3217:LMAITC%3E2.0.CO;2

Chulick, G. S., Detweiler, S., & Mooney, W. D. (2013). Seismic structure of the crust and uppermost mantle of South America and surrounding oceanic basins. *Journal of South American Earth Sciences*, *42*, 260–276. https://doi.org/10.1016/j.jsames.2012.06.002

Clinton, J. F., Cua, G., Huérfano, V., von Hillebrandt-Andrade, C. G., & Cruzado, J. M. (2006). The current state of seismic monitoring in Puerto Rico. *Seismological Research Letters*, *77*(5), 532–543. https://doi.org/10.1785/gssrl.77.5.532

Condori, C., França, G. S., Tavera, H. J., Albuquerque, D. F., Bishop, B. T., & Beck, S. L. (2017). Crustal structure of north Peru from analysis of teleseismic receiver functions. *Journal of South American Earth Sciences*, *76*, 11–24. https://doi.org/10.1016/j.jsames.2017.02.006

Cornthwaite, J., Bezada, M. J., Miao, W., Schmitz, M., Prieto, G. A., Dionicio, V., et al. (2021). Caribbean slab segmentation beneath northwest South America revealed by 3-D finite frequency teleseismic P-wave tomography. *Geochemistry, Geophysics, Geosystems*, *22*(4), e2020GC009431. https://doi.org/10.1029/2020GC009431

Diebold, J., Driscoll, N., & EW-9501 Science Team. (1999). New insights on the formation of the Caribbean basalt province revealed by multichannel seismic images of volcanic structures in the Venezuelan Basin. In *Sedimentary basins of the world* (Vol. 4, pp. 561–589). Elsevier. https://doi.org/10.1016/S1874-5997(99)80053-7

Dolan, J. F., Mullins, H. T., Wald, D. J., & Mann, P. (1998). Active tectonics of the north-central Caribbean: Oblique collision, strain partitioning, and opposing subducted slabs. *Special Papers – Geological Society of America*, 1–62. https://doi.org/10.1130/0-8137-2326-4.1

Donnelly, T. W. (1994). The Caribbean sea floor. *Caribbean geology: An introduction*, *485*, 41–60. Retrieved from http://www.redciencia.cu/geobiblio/paper/1994_Donnely_The%20Caribbean%20Sea%20Floor.pdf

Ekström, G., Nettles, M., & Dziewoński, A. M. (2012). The global CMT project 2004–2010: Centroid-moment tensors for 13,017 earthquakes. *Physics of the Earth and Planetary Interiors*, *200*, 1–9. https://doi.org/10.1016/j.pepi.2012.04.002

Escuder-Viruete, J., Valverde-Vaquero, P., Rojas-Agramonte, Y., Jabites, J., & Pérez-Estaún, A. (2013). From intra-oceanic subduction to arc accretion and arc-continent collision: Insights from the structural evolution of the Río San Juan metamorphic complex, northern Hispaniola. *Journal of Structural Geology*, *46*, 34–56. https://doi.org/10.1016/j.jsg.2012.10.008

Ewing, J., Antoine, J., & Ewing, M. (1960). Geophysical measurements in the western Caribbean Sea and in the Gulf of Mexico. *Journal of Geophysical Research*, *65*(12), 4087–4126. https://doi.org/10.1029/JZ065i012p04087

Finger, N. P., Kaban, M. K., Tesauro, M., Haeger, C., Mooney, W. D., & Thomas, M. A. (2021). Thermo-compositional model of the Cratonic Lithosphere of South America. *Geochemistry, Geophysics, Geosystems*, *22*(4), e2020GC009307. https://doi.org/10.1029/2020GC009307

García-Reyes, A., & Dyment, J. (2021). Structure, age, and origin of the Caribbean Plate unraveled. *Earth and Planetary Science Letters*, *571*, 117100. https://doi.org/10.1016/j.epsl.2021.117100

Global Volcanism Program. (2013). *Volcanoes of the World*. Smithsonian Institution. https://doi.org/10.5479/si.GVP.VOTW4-2013

Gomez, S., Bird, D., & Mann, P. (2018). Deep crustal structure and tectonic origin of the Tobago-Barbados ridge. *Interpretation*, *6*(2), T471–T484. https://doi.org/10.1190/INT-2016-0176.1

Gómez-García, Á. M., Meeßen, C., Scheck-Wenderoth, M., Monsalve, G., Bott, J., Bernhardt, A., & Bernal, G. (2019). 3-D modeling of vertical gravity gradients and the delimitation of tectonic boundaries: The Caribbean oceanic domain as a case study. *Geochemistry, Geophysics, Geosystems*, *20*(11), 5371–5393. https://doi.org/10.1029/2019GC008340

Govers, R., & Wortel, M. J. R. (2005). Lithosphere tearing at STEP faults: Response to edges of subduction zones. *Earth and Planetary Science Letters*, *236*(1–2), 505–523. https://doi.org/10.1016/j.epsl.2005.03.022

Gutscher, M. A., Malavieille, J., Lallemand, S., & Collot, J. Y. (1999). Tectonic segmentation of the North Andean margin: Impact of the Carnegie Ridge collision. *Earth and Planetary Science Letters*, *168*(3–4), 255–270. https://doi.org/10.1016/S0012-821X(99)00060-6

Hacker, B. R., Peacock, S. M., Abers, G. A., & Holloway, S. D. (2003). Subduction factory 2. Are intermediate-depth earthquakes in subducting slabs linked to metamorphic dehydration reactions? *Journal of Geophysical Research*, *108*(B1). https://doi.org/10.1029/2001JB001129

Hayes, G. P., Moore, G. L., Portner, D. E., Hearne, M., Flamme, H., Furtney, M., & Smoczyk, G. M. (2018). Slab2, a comprehensive subduction zone geometry model. *Science*, *362*(6410), 58–61. https://doi.org/10.1126/science.aat4723

Hess, H. H., & Maxwell, J. C. (1953). Caribbean research project. *The Geological Society of America Bulletin*, *64*(1), 1–6. https://doi.org/10.1130/0016-7606(1953)64[1:CRP]2.0.CO;2

Hey, R., Johnson, G. L., & Lowrie, A. (1977). Recent plate motions in the Galapagos area. *The Geological Society of America Bulletin*, *88*(10), 1385–1403. https://doi.org/10.1130/0016-7606(1977)88%3C1385:RPMITG%3E2.0.CO;2

Hosseini, K., Matthews, K. J., Sigloch, K., Shephard, G. E., Domeier, M., & Tsekhmistrenko, M. (2018). SubMachine: Web-based tools for exploring seismic tomography and other models of Earth's deep interior. *Geochemistry, Geophysics, Geosystems*, *19*(5), 1464–1483. https://doi.org/10.1029/2018GC007431

Hosseini, K., Sigloch, K., Tsekhmistrenko, M., Zaheri, A., Nissen-Meyer, T., & Igel, H. (2020). Global mantle structure from multifrequency tomography using *P*, *PP* and *P*-diffracted waves. *Geophysical Journal International*, *220*(1), 96–141. https://doi.org/10.1093/gji/ggz394

Hutchings, S. J., & Mooney, W. D. (2021). The Seismicity of Indonesia and tectonic implications. *Geochemistry, Geophysics, Geosystems*, *22*(9), e2021GC009812. https://doi.org/10.1029/2021GC009812

International Seismological Centre. (2021). *On-line Bulletin*. https://doi.org/10.31905/D808B830

James, K. H. (2006). Arguments for and against the Pacific origin of the Caribbean Plate: Discussion, finding for an inter-American origin. *Geológica Acta: An International Earth Science Journal*, *4*(1–2), 279–302. Retrieved from https://www.redalyc.org/pdf/505/50540216.pdf

Kelleher, J., & McCann, W. (1976). Buoyant zones, great earthquakes, and unstable boundaries of subduction. *Journal of Geophysical Research*, *81*(26), 4885–4896. https://doi.org/10.1029/JB081i026p04885

Kellogg, J. N., Vega, V., Stallings, T. C., & Aiken, C. L. (1995). Tectonic development of Panama, Costa Rica, and the Colombian Andes: Constraints from global positioning system geodetic studies and gravity. In P. Mann (Ed.), *Geologic and Tectonic Development of the Caribbean Plate Boundary in Southern Central America: Boulder, Colorado*, *Geological Society of America Special Paper 295*. https://doi.org/10.1130/SPE295-p75

Kerr, A. C., White, R. V., Thompson, P. M., Tarney, J., & Saunders, A. D. (2003). No oceanic plateau—No Caribbean Plate? The seminal role of an oceanic plateau in Caribbean Plate evolution. In C. Bartolini, R. T. Buffler, & J. Blickwede (Eds.), *The Circum-Gulf of Mexico and the Caribbean: Hydrocarbon habitats, basin formation, and plate tectonics: AAPG Memoir 79* (pp. 126–168). https://doi.org/10.1306/M79877C6

Kirby, S. H., Stein, S., Okal, E. A., & Rubie, D. C. (1996). Metastable mantle phase transformations and deep earthquakes in subducting oceanic lithosphere. *Reviews of Geophysics*, *34*(2), 261–306. https://doi.org/10.1029/96RG01050

Kolarsky, R. A., Mann, P., & Montero, W. (1995). Island arc response to shallow subduction of the Cocos Ridge, Costa Rica. *Special Papers – Geological Society of America*, 235. https://doi.org/10.1130/SPE295-p235

Kroehler, M. E., Mann, P., Escalona, A., & Christeson, G. L. (2011). Late Cretaceous-Miocene diachronous onset of back thrusting along the South Caribbean Deformed Belt and its importance for understanding processes of arc collision and crustal growth. *Tectonics*, *30*(6). https://doi.org/10.1029/2011TC002918

Leroy, S., Mauffret, A., Patriat, P., & Mercier de Lépinay, B. (2000). An alternative interpretation of the Cayman trough evolution from a reidentification of magnetic anomalies. *Geophysical Journal International*, *141*(3), 539–557. https://doi.org/10.1046/j.1365-246x.2000.00059.x

Lugo, J., & Mann, P. (1995). Jurassic-Eocene tectonic evolution of Maracaibo basin, Venezuela. In A. J. Tankard, R. S. Suárez, & H. J. Welsink (Eds.), *Petroleum basins of South America: AAPG Memoir 62* (pp. 699–725). https://doi.org/10.1306/M62593C38

Mann, P. (1999). Caribbean sedimentary basins: Classification and tectonic setting from Jurassic to present. *Sedimentary Basins of the World*, *4*, 3–31. https://doi.org/10.1016/S1874-5997(99)80035-5

Mauffret, A., & Leroy, S. (1997). Seismic stratigraphy and structure of the Caribbean igneous province. *Tectonophysics*, *283*(1–4), 61–104. https://doi.org/10.1016/S0040-1951(97)00103-0

Mazuera, F., Schmitz, M., Escalona, A., Zelt, C., & Levander, A. (2019). Lithospheric structure of northwestern Venezuela from wide-angle seismic data: Implications for the understanding of continental margin evolution. *Journal of Geophysical Research: Solid Earth*, *124*(12), 13124–13149. https://doi.org/10.1029/2019JB017892

Meyer, B., Chulliat, A., & Saltus, R. (2017). Derivation and error analysis of the Earth magnetic anomaly grid at 2 arc min resolution version 3 (EMAG2v3). *Geochemistry, Geophysics, Geosystems*, *18*(12), 4522–4537. https://doi.org/10.1002/2017GC007280

Meyer, R. P., Mooney, W. D., Hales, A. L., Helsley, C. E., Woollard, G. P., Hussong, D. M., et al. (1976). Project Nariño III: Refraction observation across a Leading Edge, Malpelo Island to the Colombian Cordillera Occidental. *The Geophysics of the Pacific Ocean Basin and Its Margin*, *19*, 105–132. https://doi.org/10.1029/GM019p0105

Mohammadzaheri, A., Sigloch, K., Hosseini, K., & Mihalynuk, M. G. (2021). Subducted lithosphere under South America from multi-frequency P-wave tomography. *Journal of Geophysical Research: Solid Earth*, *126*(6). https://doi.org/10.1029/2020JB020704

Montes, C., Cardona, A., Jaramillo, C., Pardo, A., Silva, J. C., Valencia, V., et al. (2015). Middle Miocene closure of the Central American seaway. *Science*, *348*(6231), 226–229. https://doi.org/10.1126/science.aaa2815

Montes, C., Rodriguez-Corcho, A. F., Bayona, G., Hoyos, N., Zapata, S., & Cardona, A. (2019). GPlates dataset for the tectonic reconstruction of the Northern Andes-Caribbean Margin. *Data in Brief*, *25*, 104398. https://doi.org/10.1016/j.dib.2019.104398

Mooney, W. D. (2015). 1.11 crust and lithospheric structure–Global crustal structure. *Seismology and Structure of the Earth: Treatise on Geophysics*, *1*, 361. Retrieved from https://moodle2.units.it/pluginfile.php/215590/mod_resource/content/1/Mooney_Global%20Crustal%20Structure_%20Treatise%20of%20geophysics.pdf

Mooney, W. D., & Kaban, M. K. (2010). The North American upper mantle: Density, composition, and evolution. *Journal of Geophysical Research*, *115*(B12), B12424. https://doi.org/10.1029/2010JB000866

Mora, J. A., Oncken, O., Le Breton, E., Ibánez-Mejia, M., Faccenna, C., Veloza, G., et al. (2017). Linking Late Cretaceous to Eocene tectonostratigraphy of the San Jacinto fold belt of NW Colombia with Caribbean plateau collision and flat subduction. *Tectonics*, *36*(11), 2599–2629. https://doi.org/10.1002/2017TC004612

Mora-Páez, H., Kellogg, J. N., Freymueller, J. T., Mencin, D., Fernandes, R. M., Diederix, H., et al. (2019). Crustal deformation in the northern Andes–A new GPS velocity field. *Journal of South American Earth Sciences*, *89*, 76–91. https://doi.org/10.1016/j.jsames.2018.11.002

Obayashi, M., Yoshimitsu, J., Nolet, G., Fukao, Y., Shiobara, H., Sugioka, H., et al. (2013). Finite frequency whole mantle P wave tomography: Improvement of subducted slab images. *Geophysical Research Letters*, *40*(21), 5652–5657. https://doi.org/10.1002/2013GL057401

Pindell, J., & Dewey, J. F. (1982). Permo-triassic reconstruction of western Pangea and the evolution of the Gulf of Mexico/Caribbean region. *Tectonics*, *1*(2), 179–211. https://doi.org/10.1029/TC001i002p00179

Pindell, J. L. (1991). Geologic rationale for hydrocarbon exploration in the Caribbean and adjacent regions. *Journal of Petroleum Geology*, *14*(2), 237–258. https://doi.org/10.1111/j.1747-5457.1991.tb00310.x

Pindell, J. L., Cande, S. C., Pitman, W. C., III, Rowley, D. B., Dewey, J. F., LaBrecque, J., & Haxby, W. (1988). A plate-kinematic framework for models of Caribbean evolution. *Tectonophysics*, *155*(1–4), 121–138. https://doi.org/10.1016/0040-1951(88)90262-4

Pindell, J. L., & Kennan, L. (2009). Tectonic evolution of the Gulf of Mexico, Caribbean and northern South America in the mantle reference frame: An update. *Geological Society, London, Special Publications*, *328*(1), 1–55. https://doi.org/10.1144/SP328.1

Poveda, E., Monsalve, G., & Vargas, C. A. (2015). Receiver functions and crustal structure of the northwestern Andean region, Colombia. *Journal of Geophysical Research: Solid Earth*, *120*(4), 2408–2425. https://doi.org/10.1002/2014JB011304

Rodriguez-Millan, I. (2014). *Gravity anomalies, geodynamic modelling and the Eastern Venezuela basin evolution* (Doctoral dissertation). Durham University. Retrieved from http://etheses.dur.ac.uk/9454/

Romito, S., & Mann, P. (2020). Tectonic terranes underlying the present-day Caribbean plate: Their tectonic origin, sedimentary thickness, subsidence histories, and regional controls on hydrocarbon resources. *Geological Society, London, Special Publications*, 504–377. https://doi.org/10.1144/SP504-2019-221

Rosencrantz, E. (1990). Structure and tectonics of the Yucatan Basin, Caribbean Sea, as determined from seismic reflection studies. *Tectonics*, *9*(5), 1037–1059. https://doi.org/10.1029/TC009i005p01037

Sallarès, V., Charvis, P., Flueh, E. R., & Bialas, J., & SALIERI Scientific Party. (2005). Seismic structure of the Carnegie ridge and the nature of the Galapagos hotspot. *Geophysical Journal International*, *161*(3), 763–788. https://doi.org/10.1111/j.1365-246X.2005.02592.x

Sallarès, V., Dañobeitia, J. J., & Flueh, E. R. (2000). Seismic tomography with local earthquakes in Costa Rica. *Tectonophysics*, *329*(1–4), 61–78. https://doi.org/10.1016/S0040-1951(00)00188-8

Sanchez, J., Mann, P., & Emmet, P. A. (2016). Late Cretaceous–Cenozoic tectonic transition from collision to transtension, Honduran Borderlands and Nicaraguan Rise, NW Caribbean Plate boundary. *Geological Society, London, Special Publications*, *431*(1), 273–297. https://doi.org/10.1144/SP431.3

Sandwell, D. T., Müller, R. D., Smith, W. H., Garcia, E., & Francis, R. (2014). New global marine gravity model from CryoSat-2 and Jason-1 reveals buried tectonic structure. *Science*, *346*(6205), 65–67. https://doi.org/10.1126/science.1258213

Schaeffer, A. J., & Lebedev, S. (2013). Global shear speed structure of the upper mantle and transition zone. *Geophysical Journal International*, *194*(1), 417–449. https://doi.org/10.1093/gji/ggt095

Simmons, N. A., Myers, S. C., Johannesson, G., & Matzel, E. (2012). LLNL-G3Dv3: Global P wave tomography model for improved regional and teleseismic travel time prediction. *Journal of Geophysical Research*, *117*(B10). https://doi.org/10.1029/2012JB009525

Smith, D. L. (1985). Caribbean plate relative motions. In *The great American biotic interchange* (pp. 17–48). Springer. https://doi.org/10.1007/978-1-4684-9181-4_2

Stolk, W., Kaban, M. K., Beekman, F., Tesauro, M., Mooney, W. D., & Cloetingh, S. (2013). High resolution regional crustal models from irregularly distributed data: Application to Asia and adjacent areas. *Tectonophysics*, *602*, 55–68. https://doi.org/10.1016/j.tecto.2013.01.022

Sun, L., Mann, P., & Bird, D. E. (2021). Integration of tectonic geomorphology and crustal structure across the active obliquely collisional zone on the island of Hispaniola, northeastern Caribbean. *Geological Society, London, Special Publications*, *504*(1), 379–400. https://doi.org/10.1144/SP504-2019-242

Sun, M., Bezada, M. J., Cornthwaite, J., Prieto, G. A., Niu, F., & Levander, A. (2022). Overlapping slabs: Untangling subduction in NW South America through finite-frequency teleseismic tomography. *Earth and Planetary Science Letters*, *577*, 117253. https://doi.org/10.1016/j.epsl.2021.117253

Syracuse, E. M., & Abers, G. A. (2006). Global compilation of variations in slab depth beneath arc volcanoes and implications. *Geochemistry, Geophysics, Geosystems*, *7*(5). https://doi.org/10.1029/2005GC001045

Syracuse, E. M., van Keken, P. E., & Abers, G. A. (2010). The global range of subduction zone thermal models. *Physics of the Earth and Planetary Interiors*, *183*(1–2), 73–90. https://doi.org/10.1016/j.pepi.2010.02.004

Tesauro, M., Kaban, M. K., Mooney, W. D., & Cloetingh, S. (2014). NACr14: A 3D model for the crustal structure of the North American Continent. *Tectonophysics*, *631*, 65–86. https://doi.org/10.1016/j.tecto.2014.04.016

van Benthem, S., Govers, R., Spakman, W., & Wortel, R. (2013). Tectonic evolution and mantle structure of the Caribbean. *Journal of Geophysical Research: Solid Earth*, *118*(6), 3019–3036. https://doi.org/10.1002/jgrb.50235

Vargas, C. A., & Mann, P. (2013). Tearing and breaking off of subducted slabs as the result of collision of the Panama Arc-Indenter with northwestern South America. *Bulletin of the Seismological Society of America*, *103*(3), 2025–2046. https://doi.org/10.1785/0120120328

Vence, E., & Mann, P. (2020). Subsurface basement, structure, stratigraphy, and timing of regional tectonic events affecting the Guajira margin of northern Colombia. *Interpretation*, *8*(4), ST69–ST105. https://doi.org/10.1190/INT-2020-0016.1

Vogt, P. R., Lowrie, A., Bracey, D. R., & Hey, R. N. (1976). *Subduction of aseismic oceanic ridges: Effects on shape, seismicity, and other characteristics of consuming plate boundaries* (Vol. 172). Geological Society of America. https://doi.org/10.1130/SPE172-p1

Wagner, L. S., Jaramillo, J. S., Ramírez-Hoyos, L. F., Monsalve, G., Cardona, A., & Becker, T. W. (2017). Transient slab flattening beneath Colombia. *Geophysical Research Letters*, *44*(13), 6616–6623. https://doi.org/10.1002/2017GL073981

Wessel, P., Smith, W. H., Scharroo, R., Luis, J. M., & Wobble, F. (2013). Generic mapping tools: Improved version released. *Eos, Transactions American Geophysical Union*, *94*(45), 409–410. https://doi.org/10.1002/2013EO450001

Zhu, H., Stern, R. J., & Yang, J. (2020). Seismic evidence for subduction-induced mantle flows underneath Middle America. *Nature Communications*, *11*(1), 1–12. https://doi.org/10.1038/s41467-020-15492-6

Reference From the Supporting Information

Seton, M., Müller, R. D., Zahirovic, S., Williams, S., Wright, N., Cannon, J., et al. (2020). A global dataset of present-day oceanic crustal age and seafloor spreading parameters. *Geochemistry, Geophysics, Geosystems*, *21*, (10). https://doi.org/10.1029/2020GC009214